

1 **Coupled Stratospheric Ozone and Atlantic Meridional Overturning**
2 **Circulation Feedbacks on the Northern Hemisphere Midlatitude Jet**
3 **Response to 4xCO₂**

4 Clara Orbe^{a,b}, David Rind^a, Darryn Waugh^c, Jeffrey Jonas^{a,d}, Xiyue Zhang^c, Gabriel Chiodo^e,
5 Larissa Nazarenko^{a,d}, and Gavin A. Schmidt^a

6 ^a *NASA Goddard Institute for Space Studies, New York, NY*

7 ^b *Department of Applied Physics and Applied Mathematics, Columbia University, New York, NY*

8 ^c *Department of Earth and Planetary Sciences, Johns Hopkins University, Baltimore, MD*

9 ^d *Center for Climate Systems Research, Earth Institute, Columbia University, New York, NY*

10 ^e *Institute for Atmospheric and Climate Science, ETH Zurich, Switzerland*

12 ABSTRACT: Stratospheric ozone, and its response to anthropogenic forcings, provide an im-
13 portant pathway for the coupling between atmospheric composition and climate. In addition to
14 stratospheric ozone’s radiative impacts, recent studies have shown that changes in the ozone layer
15 due to 4xCO₂ have a considerable impact on the Northern Hemisphere (NH) tropospheric cir-
16 culation, inducing an equatorward shift of the North Atlantic jet during boreal winter. Using
17 simulations produced with the NASA Goddard Institute for Space Studies (GISS) high-top climate
18 model (E2.2) we show that this equatorward jet shift can induce a more rapid weakening of the At-
19 lantic Meridional Overturning Circulation (AMOC), resulting in a poleward shift and acceleration
20 of the jet on longer timescales. As such, coupled feedbacks from both stratospheric ozone and the
21 AMOC result in a two-timescale response of the NH midlatitude jet to abrupt 4xCO₂ forcing: a
22 “fast” response (5-20 years) during which it shifts equatorward and a “total” response (~100-150
23 years) during which the jet shifts poleward. The latter is driven by a weakening of the AMOC
24 that develops in response to weaker surface zonal winds, that result in reduced heat fluxes out
25 of the subpolar gyre and reduced North Atlantic Deep Water formation. Our results suggest that
26 stratospheric ozone changes in the lower stratosphere can have a surprisingly powerful effect on
27 the AMOC, independent of other aspects of climate change.

28 **1. Introduction**

29 There is large uncertainty in the atmospheric circulation response to increasing greenhouse gases
30 (see Shepherd (2014) and references therein). Although models generally predict a poleward shift
31 of the midlatitude eddy-driven jet, the magnitude of this shift is highly uncertain (e.g., Vallis et al.
32 (2015); Grise and Polvani (2014)) as are its underlying drivers (Shaw (2019)). This is especially
33 true in the Northern Hemisphere (NH), where there are opposing thermodynamic influences, i.e.
34 opposite meridional temperature gradient responses at the surface versus the upper troposphere
35 (Shaw et al. (2016)). Thus, while enhanced warming in the lower polar troposphere relative
36 to the lower tropical troposphere (i.e., Arctic amplification) contributes to reduced meridional
37 temperature gradients, increases in upper tropospheric tropical warming contribute to enhanced
38 temperature gradients aloft (Butler et al. (2010); Yuval and Kaspi (2020)) and it is not clear how
39 these competing processes affect the zonal mean midlatitude jet.

40 Many processes have been shown to influence the response of meridional temperature gradients
41 to increased CO₂, including polar amplification (see Smith et al. (2019) and references therein)
42 and cloud feedbacks (e.g., Ceppi and Hartmann (2015); Voigt and Shaw (2015)). By comparison,
43 composition feedbacks associated with the ozone response to CO₂ have been less well examined
44 although stratospheric ozone changes have been identified as an important pathway coupling
45 composition to climate (Isaksen et al. (2009)). In particular, the stratospheric ozone response to
46 4xCO₂ consists of robust decreases in the tropical lower stratosphere (LS), increases in the tropical
47 upper stratosphere and increases over high latitudes (Chiodo et al. (2018)). **In the tropics, the**
48 **reductions in LS ozone are strongly correlated with the response of stratospheric upwelling (Fig.**
49 **6 in Chiodo et al. (2018))** and, while the exact details of these changes are model dependent,
50 especially over high latitudes, the general pattern is very consistent among models (e.g., Nowack
51 et al. (2015); Chiodo et al. (2018) and Chiodo and Polvani (2019) (hereafter CP2019)).

52 This pattern of reduced (increased) ozone over the tropical (high latitude) LS in response to
53 4xCO₂ has immediate implications for temperature gradients in the stratosphere by cooling the
54 tropics and warming high latitudes (Nowack et al. (2015); Chiodo et al. (2018); Li and Newman
55 (2022)). As CP2019 and Li and Newman (2022) showed, these changes in temperature gradients
56 drive an anomalous equatorward shift of the midlatitude jet in the Southern Hemisphere (SH). In
57 addition, both studies also showed shifts in the Northern Hemisphere (NH) **during boreal winter,**

58 where anomalies extend down into the lower troposphere and are concentrated over the Atlantic,
59 resembling the negative phase of the North Atlantic Oscillation (NAO). **By comparison, the ozone**
60 **feedback on the Pacific jet was shown to not be robust (CP2019).**

61 A more recent study by Zhang et al. (2023) that considered two models – **distinct from the ones**
62 **used in either CP2019 or Li and Newman (2022)** – and that differed only in their representation
63 of interactive chemistry, also showed that changes in composition can impact the sign of the NH
64 midlatitude jet response to increased CO₂. However, in contrast to CP2019, the long-term impact
65 of this composition feedback was a *poleward*, not equatorward, shift of the **zonal mean** NH jet.
66 Though not investigated in detail, this poleward shift of the jet – **expressed regionally as an eastward**
67 **extension of the Atlantic jet and a poleward shift of the Pacific jet** – was linked to changes in the
68 ocean circulation, which were not examined in CP2019. More precisely, Zhang et al. (2023)
69 noted that the Atlantic Meridional Overturning Circulation (AMOC) exhibited a stronger decline
70 in interactive simulations in which trace gases and aerosols were allowed to respond to increased
71 CO₂, relative to non-interactive simulations. Indeed, recent studies have highlighted the large
72 influence that changes in the AMOC exert on the response of the NH midlatitude jet to increased
73 CO₂ (Gervais et al. (2019)), with models featuring a larger AMOC decline also tending to **produce**
74 **a stronger and eastward extended jet over the Atlantic** (Bellomo et al. (2021); Liu et al. (2020);
75 Orbe et al. (2023)).

76 The results from Zhang et al. (2023) suggest that composition feedbacks on the NH midlatitude
77 jet may depend on the response of the ocean circulation. However, that study did not examine the
78 mechanism underlying the stronger AMOC response in the interactive chemistry simulations nor
79 did it isolate the role of ozone from influences due to other trace gases and aerosols. To this end,
80 here we hypothesize that the ozone-induced negative NAO wind anomalies reported in CP2019
81 provide a potential pathway through which stratospheric ozone changes can influence the AMOC
82 and the long-term response of the NH midlatitude jet. Our hypothesis is partly predicated on
83 results from previous studies showing that variations in the jet – namely those resembling the NAO
84 – can influence variability of the AMOC through changes in wind stress (**Marshall et al. (2001);**
85 **Zhai and Marshall (2014); Delworth and Zeng (2016)**). Modified air-sea fluxes of heat, water and
86 momentum associated with variations in the NAO alter vertical and horizontal density gradients in
87 the subpolar gyre, inducing changes in deep water formation and the AMOC (e.g., Visbeck et al.

88 (1998); Delworth and Dixon (2000)). This pathway via the NAO has been used to demonstrate
89 how sudden stratospheric warmings influence the variability of heat flux anomalies into the ocean
90 and ocean mixed layer depths in the North Atlantic (O’Callaghan and Mitchell (2014)) as well as
91 the strength of the AMOC itself (Reichler et al. (2012)).

92 Here we present results from non-interactive and fully interactive chemistry global warming
93 experiments produced with the new high-top coupled atmosphere ocean version of the NASA
94 Goddard Institute for Space Studies (GISS) climate model that were submitted to the Coupled
95 Model Intercomparison Project Phase 6 (CMIP6) (Eyring et al. (2016)). We focus on simulations
96 in which CO₂ is abruptly doubled and quadrupled in order to facilitate comparison with the results
97 presented in CP2019 and Zhang et al. (2023).

98 We begin by verifying that reduced ozone in the tropical lower stratosphere, which is captured
99 only in the interactive simulations, leads to an equatorward shift of the midlatitude jet on relatively
100 fast timescales. Then we show that the AMOC response in the interactive simulations is largely
101 associated with these ozone-driven changes in the jet, not aerosols, using new experiments in
102 which the stratospheric ozone response to 4xCO₂ is isolated from changes in other trace gases and
103 aerosols. In particular, we show that our model captures the ozone-induced negative NAO-like
104 pattern first reported in CP2019; in addition, we also find that ozone-driven changes in surface
105 friction speed further weaken the AMOC, resulting in a long-term poleward shift of the NH jet.
106 As a result, we show that both stratospheric ozone changes and the AMOC influence the NH jet on
107 distinct “fast” and “total” timescales (and in the opposite sense), comprising a coupled atmosphere-
108 ocean feedback on the NH midlatitude jet response to increased CO₂. While the former “fast”
109 feedback was documented in CP2019, the latter has, to the best of our knowledge, not been reported
110 in previous studies.

111 We begin by discussing methods in Section 2 and then present key results and conclusions in
112 Sections 3 and 4, respectively.

113 **2. Methods**

114 *a. Model and Configurations*

115 Here we use the NASA Goddard Institute for Space Studies (GISS) “Middle Atmosphere (MA)”
116 Model E2.2 (Rind et al. (2020); Orbe et al. (2020)). E2.2 consists of 102 vertical levels spanning

117 the surface up to 0.002 hPa and is run at a horizontal resolution of 2 degrees by 2.5 degrees.
118 Orographic and non-orographic gravity wave drag is parameterized following Lindzen (1987)
119 and Rind et al. (1988), producing in E2.2 a quasibiennial oscillation (QBO) that compares well
120 with observations as well as improved stratospheric polar vortex variability (Ayarzagüena et al.
121 (2020); Rind et al. (2020)). Of most relevance to this study, Orbe et al. (2020) showed that E2.2
122 produces a significantly improved representation of the Brewer-Dobson and stratospheric transport
123 circulations, compared to the lower vertical resolution CMIP6 version of ModelE (E2.1, Kelley
124 et al. (2020)), resulting in reduced biases in ozone, methane, water vapor and nitrous oxide (see
125 their Figure 1). Among the different model versions discussed in Rind et al. (2020) and Orbe
126 et al. (2020) here we focus on the “Altered-Physics” (-AP) Version (E2.2-AP) because this is the
127 configuration that was submitted to CMIP6 and presented in recent studies (Ayarzagüena et al.
128 (2020); DallaSanta et al. (2021a,b)).

129 We begin by showing the results reported in Zhang et al. (2023) using both “Non-INTeractive”
130 (NINT) (Table 1, rows 1-3) and fully interactive “One-Moment Aerosols” (OMA) (Bauer et al.
131 (2020); Table 1, rows 4-6) configurations. In the NINT configuration all trace gases and aerosols
132 are set to preindustrial values. Hence, in the 2- and 4xCO₂ NINT runs neither ozone nor other trace
133 gases (besides water vapor) change in response to increased CO₂. By comparison, the OMA 2- and
134 4xCO₂ runs capture the full nonlinear ozone response to CO₂, as well as composition feedbacks
135 associated with other trace gases and aerosols.

136 In order to isolate the role of ozone feedbacks on the circulation, we then perform experiments
137 using a linearized ozone (LINOZ) configuration (Table 1, rows 7-9). In LINOZ the **stratospheric**
138 ozone field is calculated interactively by Taylor expanding the equation of state around present-day
139 (2000–2010) values such that the ozone tendency is, to first-order, parameterized as a function of
140 the local ozone mixing ratio, temperature, and overhead column ozone (McLinden et al. (2000)).
141 Tropospheric ozone is calculated using monthly mean ozone production and loss rates archived
142 from GEOS-CHEM (Rind et al. (2014)). In contrast to NINT, therefore, the LINOZ ensemble
143 captures the influence of the ozone response to CO₂ on the large-scale circulation. Unlike OMA,
144 however, it is much more computationally efficient to run and isolates the ozone feedback from
145 feedbacks related to other trace gases and aerosols. DallaSanta et al. (2021a) previously showed

148 TABLE 1. The Model E2.2 experiments presented in this study, including preindustrial control, abrupt 2xCO₂
 149 and abrupt 4xCO₂ simulations using NINT (rows 1-3), OMA (rows 4-6) and LINOZ (rows 7-9) configurations.
 150 Four NINT abrupt 4xCO₂ ensemble members are included (row 3) in order to compare with a four member
 151 4xCO₂ ensemble produced using the LINOZ configuration (row 9). The 4xCO₂ ensemble mean LINOZ ozone
 152 response is also used to force four prescribed SST and SIC preindustrial experiments (row 10) in which all
 153 forcings other than ozone are set to preindustrial values. All coupled atmosphere-ocean simulations are run using
 154 the GISS Ocean v1 (GO1) (i.e., “-G” in CMIP6 notation).

Configuration	Ozone	CO ₂	Ensemble Size	SSTs and SICs
NINT	Preindustrial	Preindustrial	1	coupled (-G ocean)
NINT	Preindustrial	2xCO ₂	1	coupled (-G ocean)
NINT	Preindustrial	4xCO ₂	4	coupled (-G ocean)
OMA	Preindustrial	Preindustrial	1	coupled (-G ocean)
OMA	2xCO ₂	2xCO ₂	1	coupled (-G ocean)
OMA	4xCO ₂	4xCO ₂	1	coupled (-G ocean)
LINOZ	Preindustrial	Preindustrial	1	coupled (-G ocean)
LINOZ	2xCO ₂	2xCO ₂	1	coupled (-G ocean)
LINOZ	4xCO ₂	4xCO ₂	4	coupled (-G ocean)
NINT	LINOZ 4xCO ₂	Preindustrial	4	Prescribed Preindustrial

146 that the LINOZ ozone parameterization reproduces well the vertical structure and seasonal cycle
 147 of stratospheric ozone obtained from the fully interactive OMA configuration (see their Figure 1).

155 *b. Experiments*

156 For the different model configurations (NINT, OMA, LINOZ) we perform 150-year-long abrupt
 157 2- and 4xCO₂ experiments, in which CO₂ values are abruptly doubled and quadrupled relative to
 158 preindustrial concentrations. For each model configuration, these experiments are branched from
 159 a corresponding preindustrial control simulation. For NINT and LINOZ four-member 4xCO₂
 160 ensembles are run in order to assess the robustness of any ozone feedbacks. These experiments are
 161 all conducted using the atmosphere-ocean version of E2.2-AP that is coupled to the GISS Ocean
 162 v1 (GO1) (i.e., “-G” in CMIP6 notation, hereafter simply E2.2-G). For coupled atmosphere-ocean
 163 configurations in which (four-member) ensembles are run, different ensemble members are chosen
 164 from different initial ocean states spaced 20 years apart in the corresponding preindustrial control
 165 simulation.

166 In addition to the coupled atmosphere-ocean experiments, we also present results from a four-
167 member ensemble of 60-year-long atmosphere-only experiments in which sea surface temperatures
168 (SSTs) and sea ice concentrations (SICs) are fixed to preindustrial values, but the monthly mean
169 time-evolving ensemble mean ozone response from the coupled LINOZ 4xCO₂ experiments is
170 prescribed (Table 1, row 10). This allows us to quantify the impact of the ozone feedback
171 represented in LINOZ on the large-scale circulation, absent any contributions from changes in
172 background CO₂, sea ice concentrations or sea surface temperatures.

173 *c. Analysis*

174 1) TIMESCALES

175 When examining the midlatitude jet response to increased CO₂ we account for the fact that
176 extratropical circulation changes consist of distinct “fast” and “slow” responses (Ceppi et al. (2018),
177 hereafter CZS2018). More precisely, CZS2018 show that most of the shift of the midlatitude jets
178 occurs within 5-10 years of a steplike (abrupt) CO₂ forcing, with little shifts occurring during a
179 slower response over which SSTs change over subsequent decades. In contrast to the Southern
180 Hemisphere, zonal asymmetries play an important role in the Northern Hemisphere, where the
181 influence of local patterns in sea surface temperature change can result in oppositely signed jet
182 shifts **between the Pacific and Atlantic ocean basins** on “slow” timescales. Given this potential
183 for compensating jet shifts on distinct timescales, we therefore decompose the CO₂ circulation
184 response into “fast” and “total” timescale responses.

185 **More precisely, we modify the original approach used in CZS2018 to define our “fast” response as**
186 **the difference between the ensemble mean 4xCO₂ response, averaged over years 5-20 (as opposed**
187 **to years 5-10), and the corresponding preindustrial control simulation. Calculations of the “fast”**
188 **response using years 5-10 produce similar results (not shown), but the choice of years 5-20 better**
189 **accounts for the large internal variability in our runs, perhaps related to a somewhat larger ENSO**
190 **amplitude in our model compared to observations (Rind et al. (2020)).**

191 In addition, instead of focusing on the “slow” response, defined in CZS2018 as the difference
192 between averages over years 121-140 and years 5-10, here we examine the “total” response, defined
193 as the difference between the ensemble mean 4xCO₂ response, averaged over years 100-150, and the
194 preindustrial control simulation. This approach **for defining the “total” response** is not only more

195 consistent with what was used in Zhang et al. (2023) and CP2019, with which we directly compare
196 our results throughout, **but also with numerous other studies examining the atmospheric circulation**
197 **response to an abrupt quadrupling of CO₂ (e.g., Grise and Polvani (2014, 2016); Menzel et al.**
198 **(2019)).** Note that in response to an abrupt quadrupling of CO₂ the NINT model configuration
199 produces global mean surface temperature “fast” and “total” responses of ~2.9°C and ~3.9°C,
200 respectively.

201 **Statistical significance of the four-member ensemble mean LINOZ-NINT and single member**
202 **OMA-NINT abrupt CO₂ differences is assessed using a two-sample Student’s t-test at the 5%**
203 **confidence level. Significance of differences is assessed relative to the interannual variability in**
204 **the corresponding preindustrial control simulation.**

205 2) ANALYSIS FIELDS

206 In addition to the atmospheric variables examined in CP2019 (i.e., zonal mean wind, zonal mean
207 temperature, surface temperature, 850 hPa zonal wind) we examine ocean variables relevant to
208 understanding the evolution of the AMOC and its coupling to the atmosphere. In particular, in
209 addition to examining the surface mixed layer depths we also examine sea surface temperatures,
210 surface friction speed, horizontal ocean heat and salinity transports, as well as the net heat fluxes
211 which, together with the net freshwater fluxes (F; inferred from precipitation minus evaporation
212 (P-E)), provide information about the surface buoyancy forcing (Large and Yeager (2009)). In our
213 simulations, the preindustrial climatological buoyancy forcing over the North Atlantic is dominated
214 by the sum of the net heat fluxes ($Q = Q_H + Q_E + Q_S + Q_L$), which are defined to be positive into the
215 ocean (Appendix Figure A1, left). These are further partitioned into their respective latent heat
216 (Q_E) and sensible heat (Q_H) contributions as we find that the net solar (Q_S) and longwave (Q_L) flux
217 radiative contributions are negligible over the North Atlantic region (Appendix Figure A1, right).

218 Given our interest in the Northern Hemisphere **and our expectations that stratospheric ozone feed-**
219 **backs on the NH jet will occur during boreal winter (CP2019)**, we focus primarily on December-
220 January-February (DJF). The ocean heat transport changes in our simulations are also most pro-
221 nounced during DJF, consistent with the analyses presented in Romanou et al. (2023) and Orbe
222 et al. (2023).

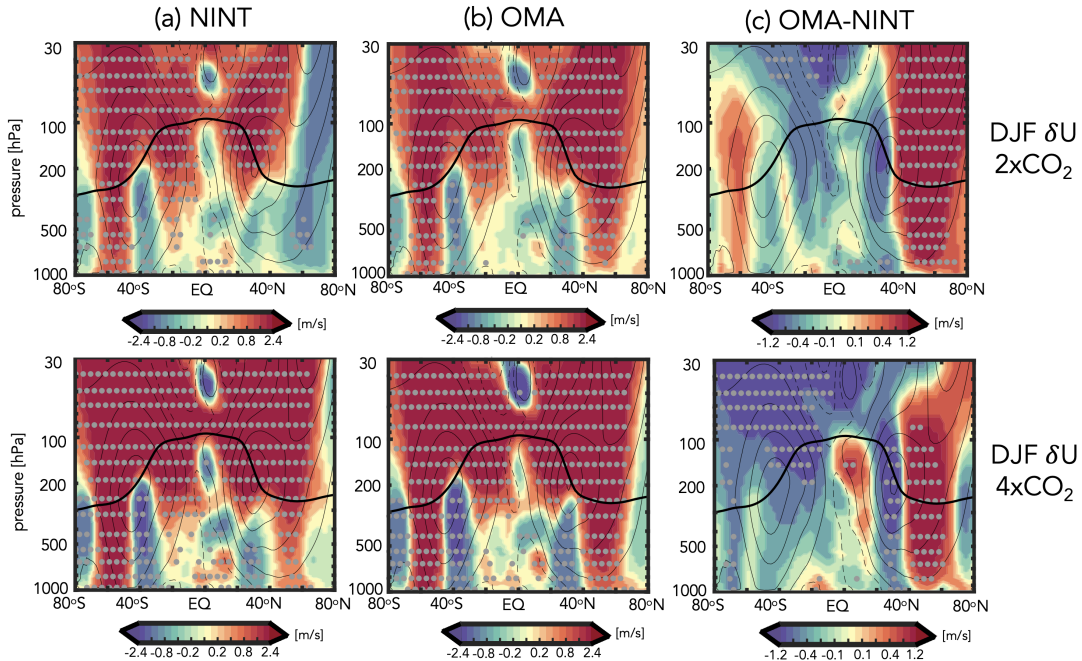
3. Results

a. Abrupt 2xCO₂ and 4xCO₂ Zonal Mean Wind Response: OMA versus NINT

Before focusing on ozone feedbacks, we first review the OMA versus NINT differences in NH jet behavior that were presented in Zhang et al. (2023) (Figure 1). In the stratosphere the zonally averaged DJF wind response to 2- and 4xCO₂ features an acceleration at nearly all latitudes, consistent with amplified warming in the tropical upper troposphere (Shaw (2019)) and increased cooling of the stratosphere with height (Garcia and Randel (2008)). Similar wind responses emerge in both the NINT and OMA configurations, except over northern high latitudes at 2xCO₂, where the zonal winds in NINT weaken and the response is not statistically significant.

In the troposphere, however, there are noticeable differences between the OMA and NINT simulations. In particular, the NH midlatitude jet features a much stronger poleward shift in OMA, compared to NINT (Figures 3 and 6 in Zhang et al. (2023)). As discussed in that study, the stronger response in OMA results in enhanced eddy mixing along isentropes on the poleward flank of the NH jet, resulting in increased transport of tracers from the northern midlatitude surface to the Arctic (not shown). This difference between OMA and NINT occurs at both 2- and at 4xCO₂, resulting in a nonlinearity in the jet (and tracer transport) response in NINT that is not present in the OMA simulations. In the SH, by comparison, the differences between OMA and NINT are much smaller and not statistically significant. Here “nonlinearity” is defined as the difference $\frac{1}{2}(\delta 4xCO_2) - \delta 2xCO_2$, consistent with its use in previous studies (e.g., Chadwick and Good (2013); Mitevski et al. (2021)).

Zhang et al. (2023) hypothesized that the nonlinearity in NH jet behavior evident in the “total” response in the NINT model configuration was related to a nonlinear AMOC response to CO₂ forcing (Figure 2). That is, despite an initial weakening, the AMOC eventually recovers to preindustrial values in the NINT 2xCO₂ simulation, in contrast to the total response to 4xCO₂ in which the AMOC is about 10 SV weaker than the preindustrial control (Fig. 2, left, black box). This results in a so-called “AMOC nonlinearity” to CO₂ forcing of ~-5SV in the NINT configuration. By comparison, in the OMA configuration, the AMOC weakens by ~7 and ~17 SV in the 2- and 4xCO₂ simulations, respectively, representing only a very weak (and not statistically

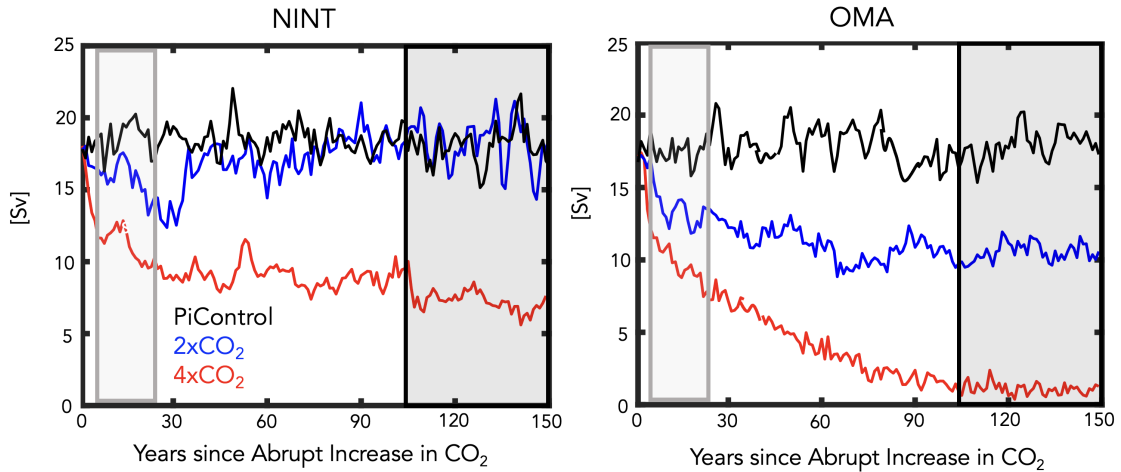


232 FIG. 1. Colors show the December-January-February (DJF) response of the zonal mean zonal winds, U , to
 233 an abrupt doubling (top) and quadrupling (bottom) of CO_2 , averaged over years 100-150. Results are shown
 234 for NINT (a,d) and fully interactive OMA configurations (b,e), where one ensemble member has been used for
 235 each forcing scenario. The OMA - NINT differences are also shown (c,f). Black contours denote climatological
 236 mean preindustrial control DJF U values (contour interval: 8 m/s). Stippled regions are statistically significant
 237 and the black thick line shows the climatological mean tropopause in the preindustrial control NINT simulation.
 238 Note that all colorbar bounds are consistent with those used in Chiodo and Polvani (2019) in order to facilitate
 239 comparisons with that study.

259 **significant**) nonlinearity in the long-term response of the AMOC (of ~ 1.5 SV) (Fig. 2, right, black
 260 box).

265 As it is difficult to meaningfully interpret the zonal mean wind response in the NH, where there
 266 are large zonal variations in the midlatitude jet (Simpson et al. (2014)), we next compare the 850
 267 hPa zonal wind changes between the NINT and OMA 4xCO₂ simulations, further distinguishing
 268 between “fast” and “total” responses (Figure 3). We begin with the NINT equilibrated or “total”
 269 response (i.e. years 100-150), which consists of a poleward jet shift over the Pacific basin and an
 270 acceleration and eastward extension of the jet over the Atlantic and Eurasia (Fig. 3b). This pattern
 271 is amplified in the OMA run (Fig. 3d), in which both the strengthening and eastward extension of

Annual Mean AMOC Response at 48°N



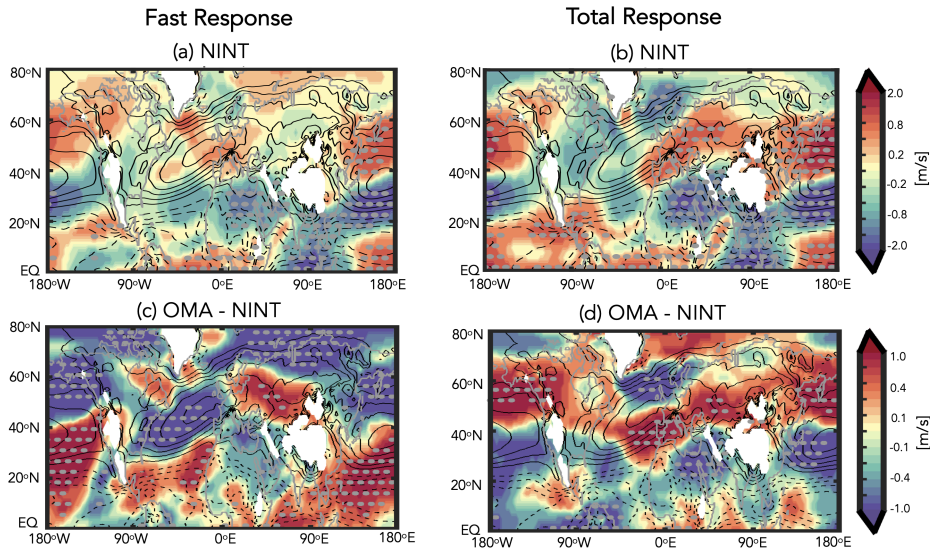
261 FIG. 2. Evolution of the annual mean maximum overturning stream function below 900m in the Atlantic ocean,
 262 evaluated at 48°N, for the preindustrial control (black), abrupt 2xCO₂ (blue) and abrupt 4xCO₂ (red) simulations.
 263 Results for the NINT (left) and OMA (right) configurations are shown. Light grey and black shaded boxes denote
 264 the “fast” and “total” timescale response averaging periods.

272 the jet over the Atlantic and its poleward shift over the Pacific are more pronounced. This amplified
 273 response in OMA over both the Pacific and Eurasia is also evident at 300 hPa (Appendix Figure
 274 A2b).

275 This wind response in OMA, relative to NINT, is consistent with the jet differences identified
 276 in Orbe et al. (2023) between two non-interactive simulations of the GISS low-top climate model
 277 in which only the AMOC strength differed. **The enhanced and eastwardly extension of the North**
 278 **Atlantic jet is also consistent with previous studies employing water hosing simulations (e.g.,**
 279 **Bellomo et al. (2023); Jackson et al. (2015).** This suggests that the jet differences between OMA
 280 and NINT on these longer timescales are primarily driven by differences in the AMOC response,
 281 as hypothesized in Zhang et al. (2023).

288 Figure 2 (grey boxes) highlights how the AMOC differences between OMA and NINT noted
 289 in Zhang et al. (2023) arise very early in the simulations (within the first 20 years). Over these
 290 years – which comprise the “fast” response – the impact of interactive chemistry on the zonal
 291 wind changes at 850 hPa is very different (Fig. 3a,c). In particular, over the Atlantic, interactive
 292 composition results in a strong weakening over the midlatitude jet core and an acceleration on the

DJF 4xCO₂ δU at 850 hPa



282 FIG. 3. Colors show the 4xCO₂ (four member) ensemble mean change in the DJF 850 hPa zonal winds
 283 for the NINT configuration, decomposed into “fast” (i.e. years 5-20) (a) and “total” (i.e. years 100-150) (b)
 284 responses. The OMA - NINT fast and total differences are shown in (c) and (d), respectively. Note that one
 285 ensemble member is used in displaying the OMA - NINT differences (same as used in Figure 1). Black contours
 286 denote climatological mean preindustrial control DJF values (U contour interval: 2 m/s) and stippled regions are
 287 statistically significant.

293 equatorward flank of the jet (Fig. 3c). This wind change is also evident at 300 hPa (not examined
 294 in CP2019), where the winds accelerate on the equatorward and poleward flanks of the midlatitude
 295 and subtropical jets, respectively (Fig. A2a). Over the Pacific, where the midlatitude jet is more
 296 vertically coherent, interactive chemistry results in an anomalous equatorward jet shift relative to
 297 the NINT simulation at both 850 hPa (Fig. 3a) and 300 hPa (Fig. A2a).

298 This fast composition feedback that occurs over years 5-20 is consistent with the results from
 299 CP2019, who showed that the ozone response to 4xCO₂ induces a weakening of the North Atlantic
 300 jet and a strengthening on its equatorward flank (see their Figure 6). This response is reminiscent
 301 of the negative phase of the NAO which previous studies have shown can result in a weaker
 302 AMOC (Delworth and Zeng (2016)). In CP2019, however, this response is realized through
 303 changes in stratospheric ozone alone, whereas in OMA all trace gases and aerosols are responding.
 304 Furthermore, the significance of this rapid response with only one ensemble member is uncertain,

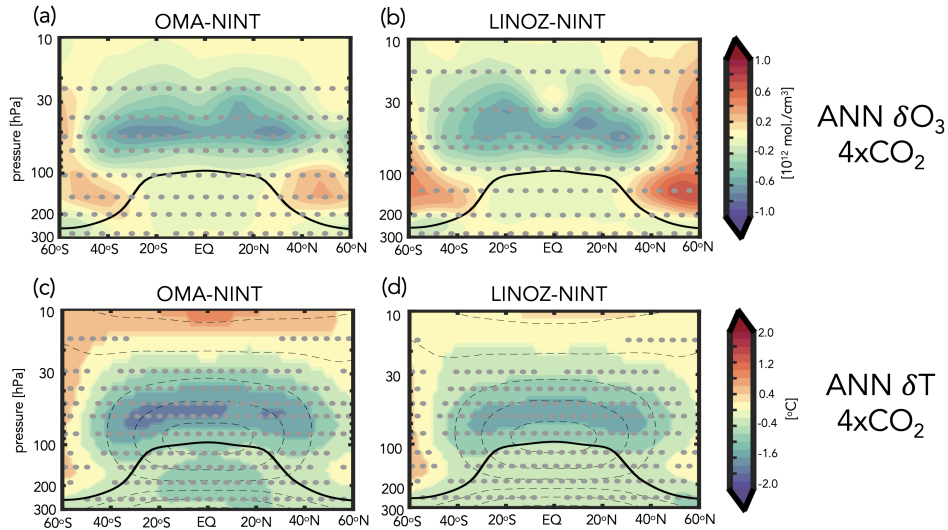
305 particularly during the first 5-20 years when the signal is confounded by large internal variability.
306 To this end, next we present results from the larger (4-member) LINOZ ensemble to examine
307 whether the fast response in the NH jet is related to stratospheric ozone changes.

308 *b. Abrupt 4xCO₂ Stratospheric Ozone and Temperature Responses: OMA versus LINOZ*

309 Before examining the circulation response in the LINOZ ensemble, we first compare the annually
310 averaged ensemble mean LINOZ 4xCO₂ ozone response with that from the OMA simulation (Figure
311 4). The amplitude and pattern of the ozone response in the LINOZ ensemble (Fig. 4b) is generally
312 very similar to the ozone response in the OMA simulation (Fig. 4a), consistent with Meraner et al.
313 (2020) who showed that the response of ozone to a quadrupling of CO₂ is well captured using
314 linearized schemes. In both OMA and LINOZ configurations the pattern of the 4xCO₂ changes
315 reflects a decrease in tropical LS ozone, associated with enhanced tropical upwelling (Garcia and
316 Randel (2008)), and enhanced concentrations over high latitudes. Over all latitudes the ozone
317 changes are statistically significant, relative to interannual variability in the preindustrial control
318 simulation.

326 Over northern high latitudes there are some differences in the mid-to-lower stratosphere (~30-100
327 hPa) between LINOZ and OMA, generally consistent with Chiodo et al. (2018), who found that
328 in this region the ozone response to CO₂ is more dependent on (nonlinear) chemical and transport
329 feedbacks and thus more likely to be captured using a more comprehensive chemistry scheme.
330 Furthermore, both simulations feature small changes in the troposphere. Overall, therefore, the
331 LINOZ scheme captures the gross characteristics of the ozone abrupt 4xCO₂ response expected
332 from previous studies. Note that most of this ozone response occurs in both simulations within the
333 5-20 years that comprise the “fast” response timescale, as shown in Chiodo et al. (2018) (see their
334 Figure 7b), although full equilibration at high latitudes does take somewhat longer (not shown).

335 In response to the ozone changes to 4xCO₂ both the OMA simulation and LINOZ ensemble
336 produce cooling in the tropical lower stratosphere and warming over high latitudes (Fig. 4c,d).
337 The amplitude of the cooling is ~1.5-2K in the tropical lower stratosphere, and is more-or-
338 less collocated with the region of largest ozone decreases. Further analysis of the temperature
339 tendencies reveals that in our model the cooler temperatures in the tropics (20°S-20°N) and the
340 warmer temperatures over high latitudes (> 40°N) are respectively associated with reduced and



319 FIG. 4. Top: Colors show the annual averaged change in ozone number density in response to $4xCO_2$. Bottom:
 320 Colors show the annual averaged change in temperature in response to $4xCO_2$, relative to the $4xCO_2$ change in the
 321 NINT simulations. Results for OMA (left) and LINOZ (right) are shown in both rows and averaged over years 5-
 322 20. One simulation is shown for OMA and the four-member ensemble mean response is shown for LINOZ. Black
 323 contours in the bottom panels show climatological mean preindustrial control temperatures (contour interval: 10
 324 C). Stippled regions are statistically significant and the black thick line shows the climatological mean tropopause
 325 in the preindustrial control NINT simulation.

341 increased radiative heating, primarily in the shortwave component (not shown). Dynamically,
 342 comparisons of the $4xCO_2$ changes in the residual mean stream function show a weaker response
 343 in LINOZ, relative to NINT (not shown). This ozone feedback on the Brewer-Dobson circulation,
 344 first identified in DallaSanta et al. (2021a), contributes to reduced upwelling, adiabatic cooling,
 345 and ozone transport within the lower tropical stratosphere. These circulation changes are therefore
 346 not the primary drivers of the temperature response; rather, they are primarily determined by the
 347 shortwave radiative response to ozone changes (CP2019).

348 The temperature responses in both OMA (Fig. 4c) and NINT (Fig. 4d) experiments are on the
 349 lower end of the 2-4K range documented in CP2019 (note that all colorbars used are consistent
 350 with that study to facilitate comparisons with their results). An important point to note is that
 351 the temperature changes due to ozone are of a similar magnitude to the temperature changes due
 352 to $4xCO_2$ alone in the tropical lower stratosphere (i.e., considering no ozone feedback), where

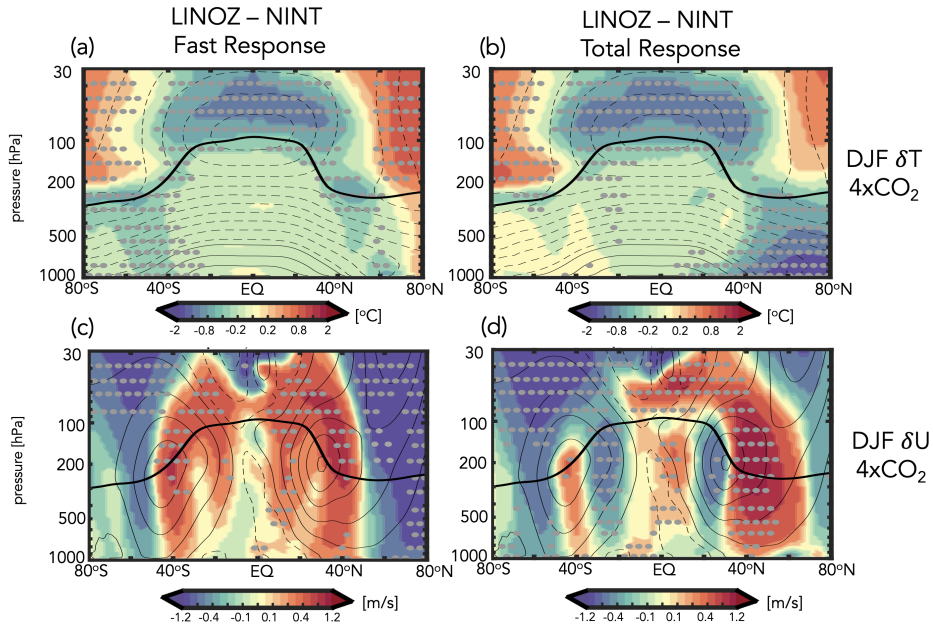
353 the stratosphere cools by $\sim 2\text{K}$ in the NINT ensemble (not shown). The ozone changes present in
354 LINOZ (and OMA) therefore represent a substantial (**same order of magnitude**) feedback on the
355 CO_2 -induced cooling in the stratosphere at this altitude.

356 *c. Ozone Feedback on Northern Hemisphere Midlatitude Jet: Fast Response*

357 The temperature response due to ozone is dynamically consequential for the troposphere to the
358 extent that it modifies temperature gradients (and winds) in the lower stratosphere. Indeed, the
359 LINOZ ensemble shows a strong **reduction** of lower stratospheric temperature gradients in both
360 hemispheres on both the fast and total response timescales (Fig. 5a,b). In the fast response, this
361 reduction in the meridional temperature gradient near the tropopause has important consequences
362 for the midlatitude jet in both hemispheres, particularly in the NH where it strengthens above and
363 along the jet core and weakens on the poleward flank of the jet over latitudes north of $\sim 50^\circ\text{N}$ (Fig.
364 5c). The winds also accelerate equatorward of the jet core, relative to NINT, in both hemispheres,
365 although the response is only statistically significant in our model in the NH. This ozone-induced
366 response in the jet is very similar to the pattern of the wind response reported in CP2019 (see their
367 Figures 4 and 5). As with the temperature changes occurring in the lower stratosphere, the wind
368 response to ozone changes is similar in magnitude to the $4\times\text{CO}_2$ response (Fig. 1), again suggesting
369 a substantial modulation of the circulation in both hemispheres by ozone changes alone.

376 **In the lower troposphere (850 hPa) the fast response evident in the zonal mean zonal winds**
377 **(Fig. 5c) is characterized by weakened winds north of 60°N over nearly all longitudes (Fig. 6a).**
378 **By comparison, the weakened wind response south of 60°N is far more zonally asymmetric. In**
379 **particular, the weakening of the midlatitude jet is concentrated over the Atlantic ocean, where**
380 **negative wind anomalies are flanked equatorward by positive wind anomalies (Fig. 6a). Time**
381 **series of the zonal winds over the North Atlantic at 300 hPa show that this anomalous weakening**
382 **of the jet in LINOZ during the first 20 years extends into the upper troposphere (Fig. A3a).**

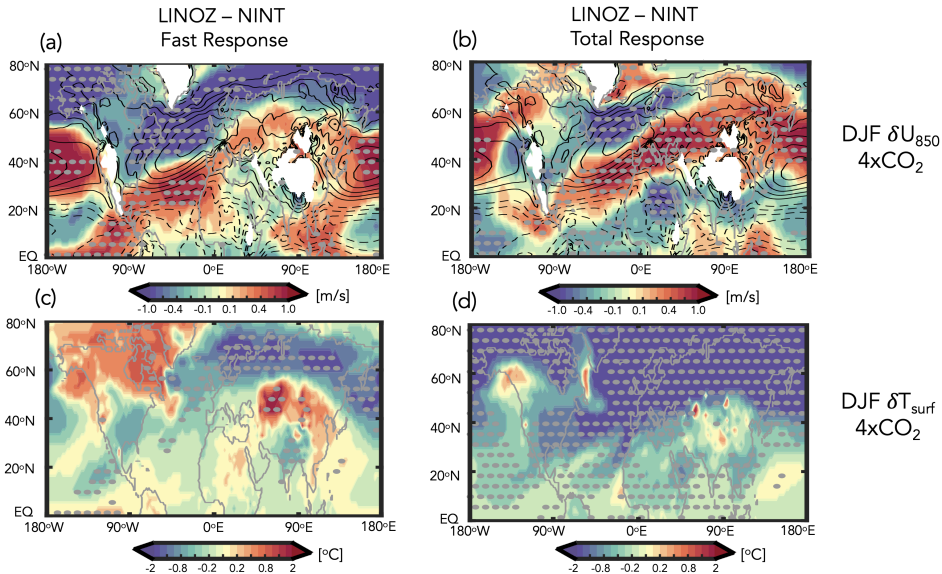
383 The LINOZ-NINT wind dipole at 850 hPa over the North Atlantic is very similar to the fast
384 wind response captured in the fully interactive OMA simulation (Fig. 3c). This consistency with
385 the response in OMA is also reflected at 300 hPa, where in both LINOZ and OMA configurations
386 the winds accelerate between the climatological subtropical and midlatitude eddy-driven jets (Fig.
387 A2a,c).



370 FIG. 5. Colors show the LINOZ-NINT ensemble mean difference in the DJF response of the zonal mean
 371 temperatures, T (top) and zonal winds, U (bottom) in response to an abrupt quadrupling of CO₂. Both LINOZ
 372 and NINT ensembles consist of four members. Responses are decomposed into “fast” (a,c) and “total” (b,d)
 373 changes. Contours denote climatological mean DJF values (T contour interval: 10 C; U contour interval: 8 m/s).
 374 Stippled regions are statistically significant and the black thick line shows the climatological mean tropopause in
 375 the preindustrial control simulation.

388 Over the Pacific, by comparison, the OMA and LINOZ responses are different, consistent with
 389 CP2019, who also found no robust ozone feedback over that sector (see their Figure 5). This
 390 lack of a robust ozone feedback over the Pacific is generally consistent with previous modeling
 391 and observational studies showing a much stronger signal of “downward” stratosphere-troposphere
 392 coupling over the Atlantic, relative to the Pacific (see Baldwin et al. (2021) and references therein),
 393 although this difference between sectors remains speculative and warrants closer inspection beyond
 394 the scope of the present study.

395 In addition to the near surface wind changes, the weakening of the North Atlantic jet in the
 396 LINOZ simulations is associated with warming over northern North America and cooling over the
 397 North Atlantic and over Eurasia, resembling the negative phase of the NAO (Fig. 6c). A similar
 398 surface temperature anomaly was identified in CP2019 (see their Figure 7) and in our model occur



401 FIG. 6. Same as Figure 5, except showing the LINOZ-NINT DJF response in the 850 hPa zonal winds, U_{850}
 402 (top) and surface temperatures, T_{surf} (bottom). Contours in top panels denote climatological mean DJF values
 403 of U_{850} (contour interval: 2 m/s). Note the similarity between the “fast” wind response shown in (a) and the
 404 CP2019 results (their Figure 6).

399 in conjunction with positive sea level pressure (SLP) anomalies over the Arctic (Appendix Figure
 400 A4, left), both features being reminiscent of a negative NAO.

405 *d. Ozone Feedback on Northern Hemisphere Midlatitude Jet: Total Response*

406 Interestingly, while the fast responses in the winds and temperatures in the LINOZ ensemble
 407 are highly consistent with the results from CP2019, our model also simulates a distinct “total”
 408 response characterized by strong cooling over the Arctic from the surface to the mid-to-upper
 409 troposphere (Fig. 5b). This cooling, which was not identified in CP2019, results in enhanced
 410 mid-to-lower tropospheric temperature gradients, prompting a strong **acceleration of the winds at**
 411 **50°N exceeding 2 m/s (Fig. 5d). Note that this acceleration at 50°N does not occur during the fast**
 412 **response, during which the winds weaken poleward up to 80°N (Fig. 5c).**

413 Zonally, the cooling over the Arctic occurring in the LINOZ ensemble during the total response
 414 primarily reflects hemispheric-wide cooling over the Arctic associated with an expansion of the
 415 North Atlantic Warming Hole (Fig. 6d, Zhang et al. (2023)). Thus, while both fast and total

416 responses feature a similar weakening of the winds over the North Atlantic, this enhancement of
417 meridional temperature gradients in the lower and mid troposphere drives a eastward extension
418 and acceleration of the Atlantic jet over Europe and a poleward shift over the Pacific ocean during
419 the total response (Fig. 6b). Time series of the zonal winds over Europe and the Pacific at 300 hPa
420 clearly show that the strengthening of the midlatitude jet in LINOZ occurring on longer timescales
421 extends into the upper troposphere (Fig. A3b).

422 By comparison, the eastward extension of the Atlantic jet is not evident during the fast response,
423 nor is the poleward shift over the Pacific. This distinct behavior of the jet over the Pacific and
424 Europe during the total response was also not captured in CP2019 and, as such, comprises a
425 coupled ozone-ocean feedback that is distinct from what was reported in that study.

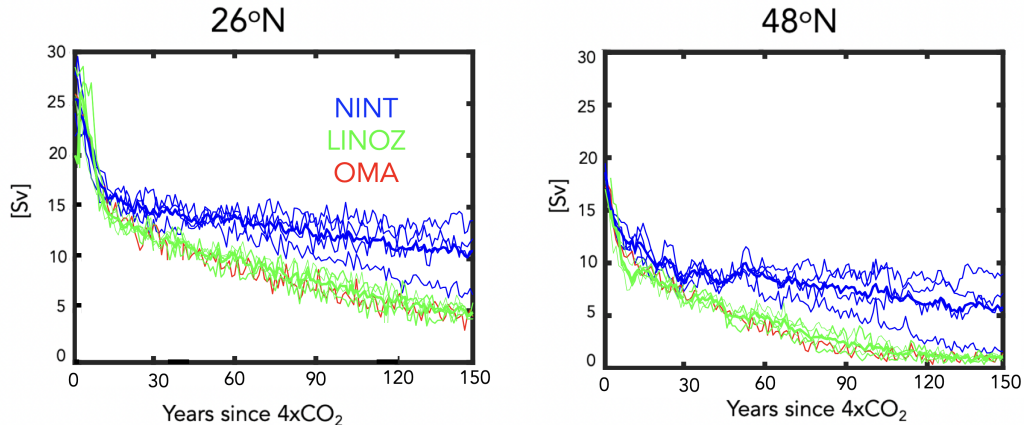
426 *e. Total Ozone Feedback: Modulation by the AMOC*

427 The “total” responses in the tropospheric winds and temperatures that occur in the LINOZ
428 ensemble are not obviously linked to ozone-driven temperature changes in the stratosphere, which
429 do not extend into the troposphere. What, then, is the driver of the lower tropospheric high latitude
430 cooling, if it is not directly linked to ozone-driven stratospheric temperature changes?

431 As expected from the OMA and NINT results presented in Zhang et al. (2023) and summarized
432 in Figure 2, we find that the strong cooling that occurs over the NH in the total LINOZ response is
433 also related to a weakening of the AMOC at $4xCO_2$ (Mitevski et al. (2021); Orbe et al. (2023)). In
434 particular, Figure 7 shows stronger weakening of the AMOC in the LINOZ (green lines) ensemble,
435 relative to NINT (blue lines) at both $26^\circ N$ (left) and at $48^\circ N$ (right). Despite large internal
436 variability, the LINOZ ensemble shows a more rapid decline of the AMOC, a difference that is
437 evident at both latitudes.

442 Interestingly, comparisons of the AMOC behavior in LINOZ with the fully interactive OMA
443 simulation (red line) shows a striking similarity (and the mechanism of these changes is also similar,
444 as shown in Section 3f). This similarity is surprising, given that other (non-ozone) trace gases and
445 aerosols are also evolving in the OMA experiment. In particular, Rind et al. (2018), using a previous
446 version of the model, observed an indirect effect of natural aerosols (primarily sea salt) on AMOC
447 stability. They showed that aerosols enhanced the local cooling of SSTs in regions of increased
448 cloud cover in a warmer climate by acting as condensation nuclei and thereby raising cloud optical

Annual Mean 4xCO₂ AMOC Response

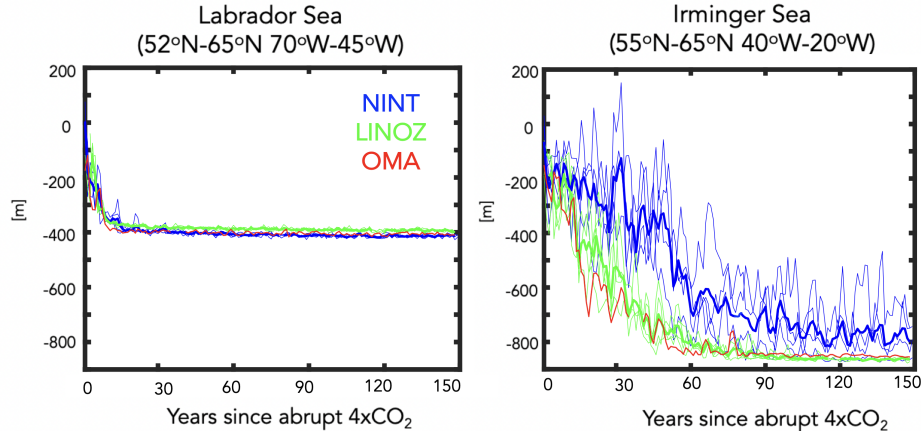


438 FIG. 7. Evolution of the annual mean maximum overturning stream function below 900 m in the Atlantic ocean,
439 evaluated at 26°N (left) and 48°N (right) in response to 4xCO₂. Results for the LINOZ and NINT ensembles are
440 shown in green and blue, respectively (thick lines denote ensemble means). Red lines show the response in the
441 OMA simulation.

449 thickness and ocean surface cooling. This surface cooling was then linked to reduced evaporation
450 relative to precipitation, resulting in anomalously positive surface freshwater forcing and reduced
451 North Atlantic Deep Water (NADW) production. That study, however, focused on aerosol-induced
452 AMOC cessations occurring on multicentennial timescales long after the initial (abrupt) warming.
453 By comparison, the results in Figure 7 identify an impact of ozone on the AMOC that occurs within
454 the first 20 years of the initial CO₂ forcing – that is, over the period during which ozone is also
455 rapidly evolving (Chiodo et al. 2018) and stratospheric temperature gradients are most impacted
456 by changes in ozone (not aerosols). Our results, therefore, highlight that during this time frame the
457 AMOC can be as (if not more) sensitive to wind-driven buoyancy changes forced by stratospheric
458 ozone anomalies as they are to aerosol-induced changes in freshwater forcing.

459 Before elucidating the mechanism of the AMOC changes in the LINOZ ensemble, we first
460 identify the region over which the largest differences in mixed layer depth begin to emerge between
461 the LINOZ (OMA) and NINT simulations. In particular, the weaker AMOC in the LINOZ and
462 OMA runs is found to be accompanied by a rapid reduction in mixed layer depths, which occur
463 primarily in the Irminger Sea region (55°N-65°N, 40°W-20°W) (Figure 8). The mixed layer depth

DJF 4xCO₂ Response in Mixed Layer Depth



471 FIG. 8. Changes in the DJF mixed layer depths, evaluated over the Labrador Sea (left) and Irminger Sea
 472 (right) in response to 4xCO₂, relative to the preindustrial control simulations. Results for the LINOZ and NINT
 473 ensembles are shown in green and blue, respectively (thick lines denote ensemble means). Red lines show the
 474 response in the OMA simulation.

464 differences among the configurations in the Labrador Sea are, by comparison, negligible. East of
 465 the Irminger Sea (i.e., 55°N–65°N, 20°W–0°) we also identify differences between the ensembles
 466 (not shown), but these emerge later, suggesting that the Irminger Sea changes are likely the initiators
 467 of the differences in AMOC behavior between the NINT and LINOZ ensembles. The same region
 468 was identified in Romanou et al. (2023) as being key for determining the sensitivity of the AMOC in
 469 various SSP 2-4.5 ensemble runs, albeit for simulations conducted using the low-top GISS climate
 470 model.

475 *f. Ozone Feedback Dependence on the AMOC: Linking Fast and Total Responses*

476 Is the fact that the AMOC declines more rapidly in the LINOZ ensemble – and the OMA
 477 simulation – a response to the ozone changes in those simulations or just a coincidence? In the fast
 478 response the zonal wind changes over the North Atlantic reflect a weakening of the jet core that is
 479 flanked equatorward by positive anomalies, resembling a negative NAO pattern. Indeed, a negative
 480 (positive) NAO has been associated with a weaker (stronger) AMOC in idealized climate model
 481 experiments in which heat is artificially added (extracted) to/from the subpolar gyre, resulting in

482 reduced (increased) NADW formation (Delworth and Zeng (2016)). Here we argue that such a
483 mechanism is present in our model simulations, resulting in a long-term modulation of the NH
484 midlatitude jet by ozone that occurs indirectly through changes in the AMOC.

485 In particular, Figure 9 shows maps of the surface zonal wind, surface friction speed, mixed layer
486 depth, net heat fluxes, sea surface temperatures, and north-south heat and salinity ocean transports,
487 averaged over years 1-5 (averages over years 5-20 are shown in Figure 10). In response to an abrupt
488 quadrupling of CO₂, the surface winds weaken over the subpolar North Atlantic region in NINT,
489 leading to a weak acceleration of the zonal winds on the poleward flank of the North Atlantic jet
490 (~60°N-70°N) (Fig. 9a, top). Over the subpolar North Atlantic the weakening of the surface winds
491 leads to a significant reduction in surface friction speed (Fig. 9b, top) and mixed layer depths (Fig.
492 9c, top), as well as increased heat flux into the ocean (in the form of reduced latent heat fluxes
493 out of the ocean) (Fig. 9d, top) and warmer sea surface temperatures (Fig. 9e, top). The reduced
494 surface density during the first 20 years associated with these warmer temperatures lead to a rapid
495 decrease in mixed layer depth by some 200 m (Figure 8) and the overturning circulation by ~ 40%
496 (Figure 7) in NINT. At these early years the changes in meridional heat and salinity transports over
497 the Irminger Sea are relatively small (Fig. 9fg, top).

498 However, in response to the ozone changes captured in the LINOZ ensemble during years 1-5,
499 there is an even stronger reduction in the surface zonal winds and friction speed (Fig. 9 ab, bottom),
500 consistent with the negative NAO response evident in the 850 hPa zonal winds (Fig. 6a). The
501 surface friction changes align closely with the reduced mixed layer depths which extend well into
502 the Irminger Sea region and over latitudes further south of the subpolar gyre (Fig. 9c, bottom).

503 The reductions in mixed layer depth that occur over the Irminger Sea are likely driven by the
504 reductions in surface wind speed which increase (primarily latent) heat fluxes into the ocean (Fig.
505 9d, bottom), driving warmer sea surface temperatures in LINOZ, relative to NINT (Fig. 9e,
506 bottom). The sign of the response of the heat fluxes in the subpolar gyre region is consistent with
507 previous studies showing that a positive (negative) phase of the NAO implies reduced (enhanced)
508 atmosphere to ocean heat fluxes (Delworth et al. (2017)). Furthermore, the spatial pattern of
509 the heat flux response is very similar to the NAO heat flux composites that were prescribed in
510 Delworth and Zeng (2016) and inferred from observations in Ma et al. (2020) (see their Figure

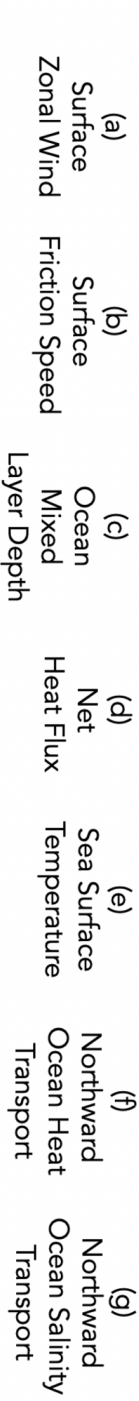
511 6), who showed that there is much greater heat loss from the ocean over the subpolar region in
512 association with a jet strengthening.

513 At the same time, the changes in freshwater forcing (P-E) during this time period are negligible
514 such that the net buoyancy forcing comprising the sum of both net heat and freshwater fluxes ($\sim Q+F$)
515 is positive. This stabilizing buoyancy forcing from surface warming makes the mixed layer depths
516 shallower by suppressing convective mixing, shutting down NADW production (Alexander et al.
517 (2000); Kantha and Clayson (2000)). There is also an initial change in the north-south heat and
518 salt transports that is colocated with the dipole anomaly in the surface friction speed, promoting
519 anomalous poleward salt and heat transport into the subpolar gyre (Fig. 9fg, bottom). This feature
520 is confined to the top few ocean layers (not shown) and the implied anomalous heat transport could
521 be contributing to the warmer sea surface temperatures in that region, in addition to the surface
522 heat flux changes.

531 Over the ensuing years (5-20) a similar pattern is maintained in the LINOZ ensemble (Figure
532 10, middle row). The reduction in NADW, however, results in reduced northward heat and salinity
533 transports (Fig. 10 fg, middle) throughout the ocean column. While this results in cooler SSTs
534 south of the subpolar gyre region (Fig. 10e, middle), which otherwise might enhance the density
535 of the near-surface water masses, the reduced northward salinity transports prevent the AMOC
536 from restarting. Interestingly, the results from the OMA simulation show a very similar response
537 as the LINOZ ensemble (Figure 10, bottom row), suggesting that stratospheric ozone changes in
538 that simulation are also likely the primary driver of the weaker AMOC in that model configuration.
539 This sequence of processes linking the surface wind changes to anomalous heat fluxes and reduced
540 NADW is basically identical to what is outlined in Figure 4 of Delworth and Zeng (2016) and
541 Figure 1 of Khatri et al. (2022). Additional analysis of the 2xCO₂ simulations, which feature a
542 stronger AMOC decline in OMA (and LINOZ) compared to NINT (Figure 2), reveals that a similar
543 mechanism for reduced NADW production occurs at lower CO₂ forcing (not shown).

547 Examining the timescale of the responses of the variables shown in Figures 9 and 10 reinforces
548 the strong coupling between the changes in surface friction speed, sea surface temperature, latent
549 heat fluxes and mixed layer depth changes over the Irminger Sea region (Figure 11a-d). Despite
550 large internal variability, there is a clear separation between the LINOZ (and OMA) and NINT
551 ensembles that emerges around year 15 (black dashed lines). The changes in sensible heat emerge

DJF 4xCO₂ Response over Years 1-5

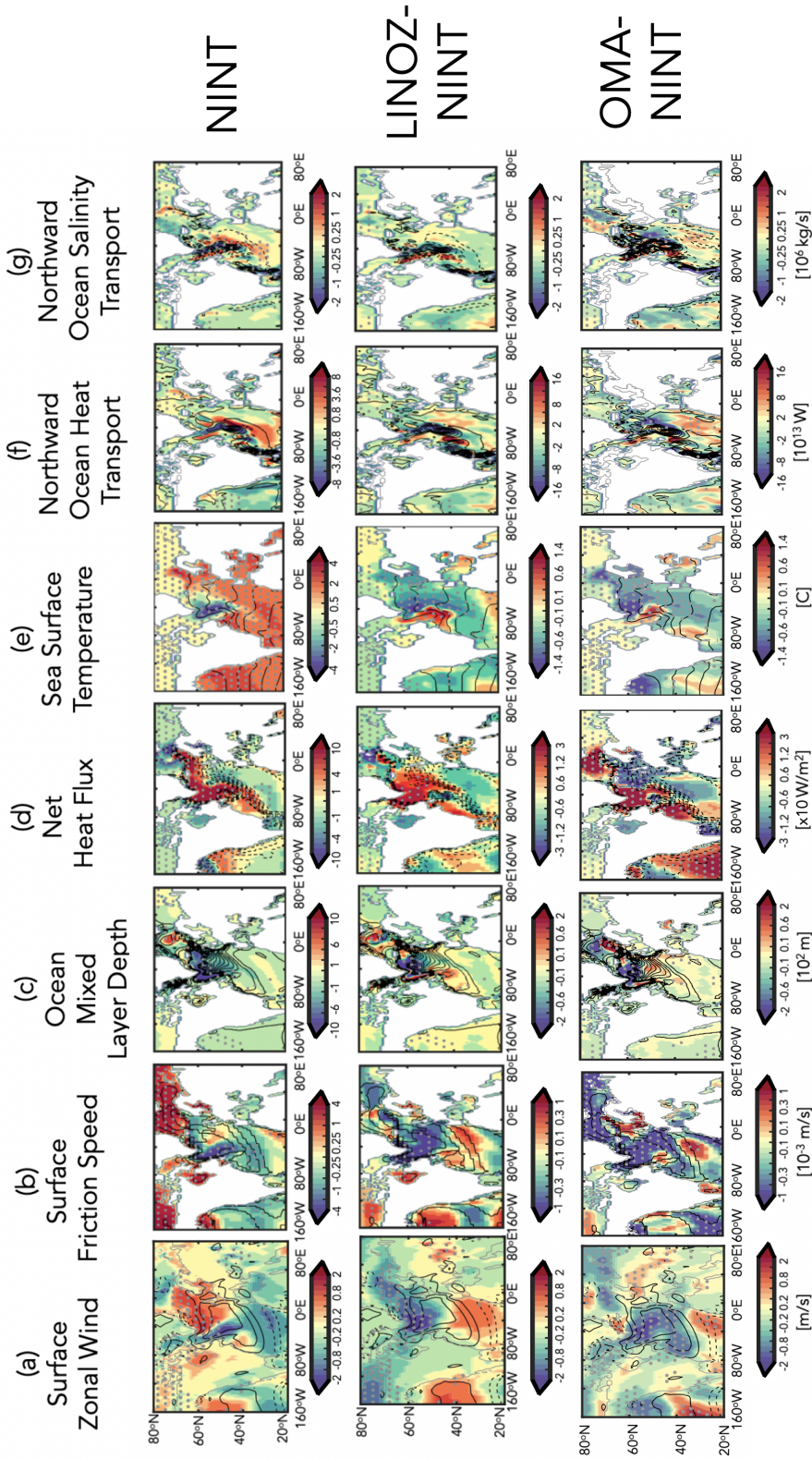


LINOZ-NINT

NINT

523 Fig. 9. Top panels: Colors show the December-January-February (DJF) response of the surface zonal wind (a), surface friction speed (b), ocean
 524 mixed layer depth (c), net heat flux (sum of sensible plus latent heat) (d), sea surface temperature (e) and northward heat (f) and salt (g) transports in
 525 response to an abrupt quadrupling of CO₂. Results are shown for the 4-member ensemble averaged NINT configuration. Bottom panels: Same as top
 526 panels, except showing the LINOZ minus NINT ensemble mean difference. For both top and bottom panels, responses have been averaged over years
 527 1-5 since “branching” from the preindustrial control simulation. Stippled regions are statistically significant and black contours denote climatological
 528 mean preindustrial control DJF values. Contour intervals: surface zonal wind [2 m/s], surface friction speed [2.5x10⁻³ m/s], mixed layer depth [60 m],
 529 net heat flux [30 W/m²], sea surface temperature interval [2 C], northward heat flux [2x10¹² W], and northward salt flux [10⁶ kg/s]. The black box in
 530 (a) bounds the Irminger Sea region over which the spatial averages in Figure 8b and Figure 11 are evaluated.

DJF 4xCO₂ Response over Years 5-20



544 Fig. 10. Same as Figure 9, except showing the responses, averaged over years 5-20. An extra row at the bottom has been added, showing the OMA -
 545 NINT differences, where the ensemble members shown in Figures 1, 2 and 3 have been used. Same contour intervals and colorbars have been used as
 546 in Fig. 9.

552 after the latent heat fluxes (Fig. 11e), suggesting that the latter play a more important role in
553 initializing the heat flux differences in LINOZ (and OMA), relative to NINT.

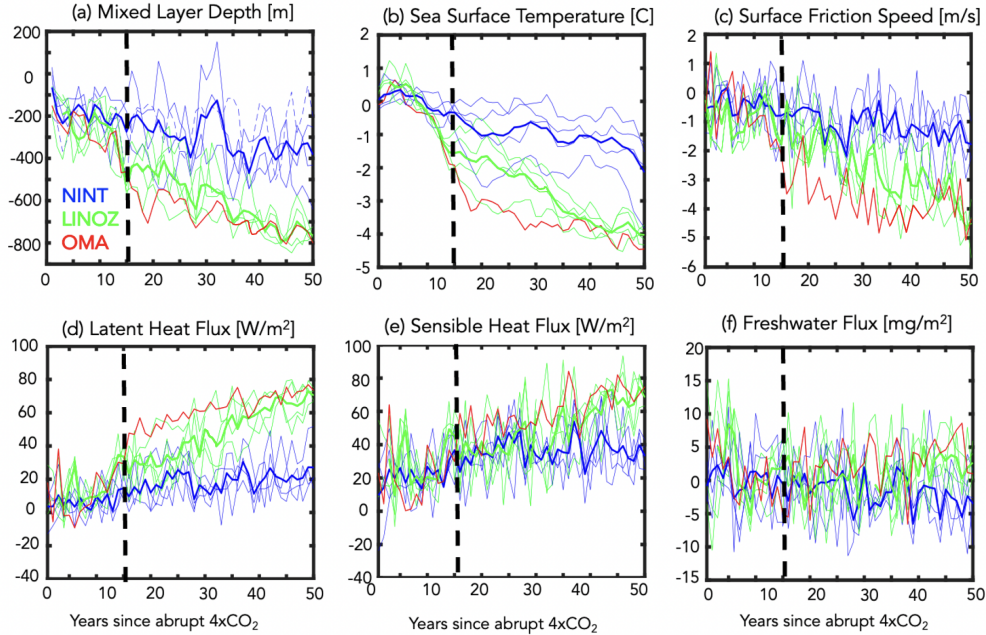
554 Finally, while they may contribute to enhanced positive buoyancy forcing later in the integrations,
555 the freshwater forcing anomalies ($F = P - E$) are shown to be negligible during the initial years
556 following the abrupt quadrupling of CO_2 (Fig. 11f), indicating that the primary driver of the
557 initial difference between the LINOZ (and OMA) and NINT runs is related to the surface wind-
558 driven changes as they impact the latent heat fluxes into the ocean. This is consistent with Roach
559 et al. (2022) who showed a much stronger correlation between AMOC strength at 26°N and the
560 heat component of the surface buoyancy flux, relative to the freshwater component, in various
561 experiments using the Community Earth System Model version 1 (CESM1) in which the winds
562 over the subpolar gyre were nudged to reanalysis values. Note that in our model other potential
563 contributors to freshwater forcing from sea ice do reveal differences between the LINOZ, OMA
564 and NINT ensembles, but these emerge several years (i.e., years $\sim 20-30$) after the changes in sea
565 surface temperatures and heat fluxes (not shown).

576 *g. Ozone Driver of AMOC Changes: Fixed SST and SIC Results*

577 So far, we have shown that the stratospheric ozone changes that occur in response to $4\times\text{CO}_2$
578 result in a negative NAO response over the North Atlantic (Fig. 5,6). In our model this triggers a
579 more rapid decline of the AMOC (Fig. 7) through surface-wind driven changes in heat fluxes into
580 the ocean (Fig. 9,10). While the time series analysis (Fig. 11) reveals that the AMOC changes
581 in the LINOZ (OMA) ensemble occur on similar timescales as the wind (and heat flux) changes,
582 one potentially confounding factor is the fact that the AMOC reduction itself results in reduced
583 wind speeds over the subpolar gyre region. These reduced near-surface winds are associated with
584 an anomalous anticyclonic flow pattern (Fig. A4, right; also discussed in Gervais et al. (2019);
585 Romanou et al. (2023); Orbe et al. (2023)), which could contribute to the reduced heat fluxes and
586 subsequent changes in NADW production. Therefore, to more convincingly link the surface wind
587 speed changes to the stratospheric ozone changes aloft, we next examine results from the fixed
588 preindustrial control SST and SIC experiments.

589 Figure 12 shows the ozone-induced zonal wind and temperature changes averaged over the last
590 twenty years of the fixed preindustrial control SST and SIC experiments in which the time-varying

DJF 4xCO₂ Response over Irminger Sea



566 FIG. 11. Changes in the DJF mixed layer depths (a), sea surface temperatures (b), surface friction speed (c),
 567 latent heat fluxes (d), sensible heat fluxes (e) and precipitation minus evaporation (f) in response to 4xCO₂,
 568 relative to the preindustrial control simulations. Averages are performed over the Irminger Sea (55°N-65°N,
 569 40°W-20°W) and the x-axis is restricted to years 1-50 in order to highlight the fast timescales on which the mixed
 570 layer depths, surface friction speed and heat fluxes evolve together. Results for the LINOZ and NINT ensembles
 571 are shown in green and blue, respectively (thick lines denote ensemble means). Red lines show the response in
 572 the OMA simulation. Black vertical lines indicate year ~15 at which point the mixed layer depth responses in
 573 the LINOZ and NINT ensembles diverge. Note that the freshwater flux unit of 1 mg/m² per second ($\equiv 0.0864$
 574 mm/day $\equiv 3.1$ cm/year) is used, because at 5°C it contributes approximately the same ocean density flux as the
 575 heat flux unit of 1 W/m² (Large and Yeager (2009)).

591 zonally varying ozone from the 4xCO₂ LINOZ ensemble is prescribed (Fig. 12 a,b). Recall that in
 592 the fixed SST and SIC experiments, only the ozone evolution differs from the preindustrial control
 593 simulation, as CO₂, SSTs and SIC are all set to preindustrial values. Comparisons with results
 594 from the fully coupled LINOZ “fast” response (see Fig. 5a,c) reveal a very similar picture. This
 595 similarity between the fully coupled fast response and the fixed preindustrial control SST and SIC

596 experiments is striking, both featuring a similar change in the NH jet associated with reduced
597 temperature gradients in the lower stratosphere as first reported in CP2019.

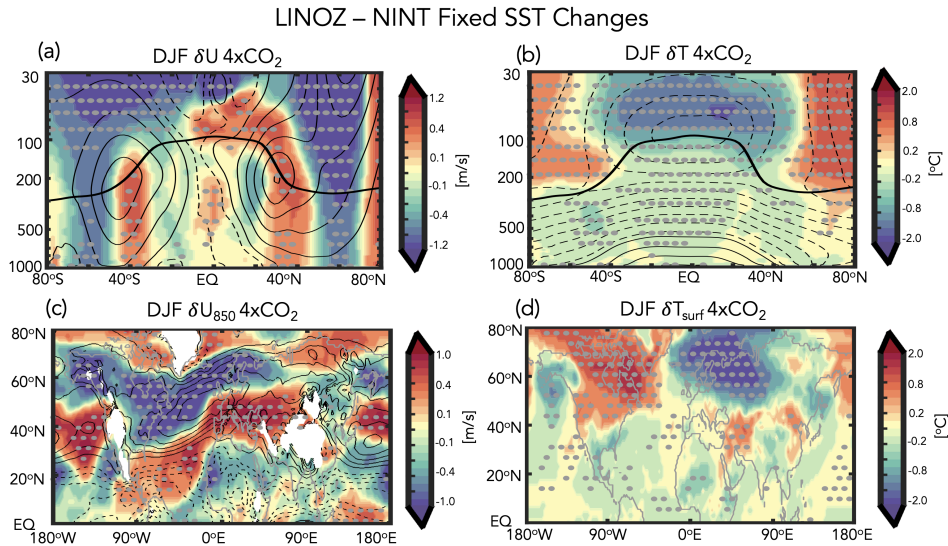
598 Comparisons of the 850 hPa zonal winds and surface temperatures over the North Atlantic
599 (Fig. 12c,d) also reveal a strikingly similar response between the fully coupled ensemble and the
600 fixed preindustrial control SST and SIC experiments (compare with Fig. 6a,c). Over the Atlantic
601 this similarity also holds aloft in the zonal wind response at 300 hPa (Fig. A3e) and in the sea
602 level pressure response (Fig. A4, bottom). The consistency in the sea level pressure changes is
603 interesting as it suggests that over the North Atlantic stratospheric ozone changes alone can result
604 in a significant reduction in the near surface winds that is on the same order (if not larger than)
605 the 4xCO₂ response. In our coupled atmosphere-ocean model this additionally results in heat
606 flux changes that are large enough to reduce NADW production, resulting in a significant (i.e.
607 ~30-40%) long-term change in AMOC strength.

608 Finally, though not reported in depth here, we have performed an additional four-member en-
609 semble that is identical to the fixed SST and SIC runs, with respect to external forcings (i.e.,
610 preindustrial background CO₂, LINOZ 4xCO₂ O₃), except run using the coupled atmosphere-
611 ocean model. Preliminary analysis of these experiments (not shown) reveals very consistent ozone
612 feedbacks on stratospheric temperatures, zonal mean winds and 850 hPa zonal winds, as captured
613 in the coupled LINOZ 4xCO₂ simulations. The responses in surface winds, net heat fluxes into
614 the ocean and mixed layer depths are also well captured, but somewhat weaker in the absence of
615 background 4xCO₂ changes. This result is not surprising and suggests that the sensitivity of the
616 AMOC to stratospheric ozone feedbacks depends partly on the background CO₂ forcing of the
617 ocean. This dependence will be explored in more depth in future studies.

626 4. Conclusions

627 Here we have used the NASA GISS coupled atmosphere-ocean high-top model (E2.2-G) to
628 examine how coupled changes in stratospheric ozone and the ocean circulation both influence the
629 abrupt 4xCO₂ response of the NH midlatitude jet. Our key results are as follows:

- 630 • The NH midlatitude jet response to 4xCO₂ is modulated by coupled feedbacks from both
631 stratospheric ozone and the AMOC, which occur on “fast” (5-20 year) and “total” (100-150
632 year) timescales, respectively.



618 FIG. 12. Top panels: Colors show the $4xCO_2$ ensemble mean response in zonal mean zonal winds, U (a),
 619 temperatures, T (b), 850 hPa zonal winds, U_{850} (c) and surface temperature, T_{surf} (d) in the prescribed SST and
 620 SIC experiments in which the time-evolving $4xCO_2$ ensemble mean LINOZ ozone response is prescribed. Note
 621 that SSTs, SICs and background CO_2 are all set to preindustrial values. Averages are shown over the last 20 years
 622 (years 40-60) of the integrations. Black contours, where shown, denote climatological mean preindustrial control
 623 DJF values (U contour interval: 8 m/s; T contour interval: 10 C; U_{850} contour interval: 2 m/s). Stippled regions
 624 are statistically significant and the black thick line in the top panels shows the climatological mean tropopause in
 625 the preindustrial control simulation.

- 633 • In the “fast” response, the zonal mean jet weakens (strengthens) on its poleward (equatorward)
 634 flank, consistent with reduced LS temperature gradients associated with ozone loss in the
 635 tropics. **This response is zonally asymmetric and is expressed as a negative NAO-like pattern,**
 636 **consisting of weaker zonal surface winds over the North Atlantic, as reported in CP2019.**
- 637 • The weaker winds over the North Atlantic **occurring during the “fast” response** are associated
 638 with increased (primarily latent) heat fluxes into the ocean, which initially result in warmer
 639 SSTs over the subpolar gyre region, reducing NADW production and leading to more rapid
 640 weakening of the AMOC.
- 641 • A reduced AMOC leads to widespread cooling over the Arctic which enhance mid-to-lower
 642 tropospheric temperature gradients, resulting in a **eastward acceleration of the Atlantic jet and**

643 a poleward shift of the Pacific jet. The regional pattern of this “total” response is consistent
644 with previously reported impacts of a weakened AMOC on the NH midlatitude jet (e.g.,
645 Bellomo et al. (2021); Liu et al. (2020); Orbe et al. (2023); Zhang et al. (2023)).

646 Taken together, the findings listed above indicate that the stratospheric ozone feedback on the NH
647 midlatitude jet reported in CP2019 is coupled to the behavior of the AMOC during the “fast”
648 response, wherein the jet weakens over the North Atlantic. In our model, this wind response
649 extends to the surface, resulting in reduced heat fluxes out of the subpolar gyre region and a more
650 rapid decline of the AMOC. On longer timescales, these changes in the AMOC subsequently
651 drive a poleward shift in the NH midlatitude jet. Unlike the “fast” response, this “total” timescale
652 response in the NH jet to changes in stratospheric ozone has not been previously reported, to the
653 best of our knowledge. This may reflect differing sensitivities of the AMOC among models and
654 our results will, of course, need to be tested using other models to assess robustness.

655 Another intriguing result from this study is that the stronger decline of the AMOC in the LINOZ
656 ensemble does not appear to be a coincidence. Rather, in our model, the “fast” ozone and “total”
657 AMOC feedbacks on the NH jet are coupled through surface-wind driven changes in heat fluxes
658 into the ocean. Key here is the fact that this sensitivity in the AMOC is driven only by changes in
659 stratospheric ozone, which we have isolated from changes in other trace gases and aerosols.

660 This last point is important to note, as previous studies have long shown that interactive atmo-
661 spheric composition can strongly influence the AMOC, but place an almost exclusive focus on the
662 role of aerosols (Booth et al. (2012); Cowan and Cai (2013); Swingedouw et al. (2015); Zhang et al.
663 (2013, 2019); Robson et al. (2022)). In particular, Rind et al. (2018) identified a larger sensitivity
664 of the AMOC response to global warming using an interactive configuration of the CMIP5 version
665 of the GISS climate model (GISS-E2-R), compared to a non-interactive version. In that study, mul-
666 tacentennial cessations of the AMOC were found to occur in simulations in which natural aerosols
667 (primarily sea salt) were allowed to locally cool sea surface temperatures through their influence
668 on cloud optical thickness; these cooler SSTs were then linked to reduced evaporation relative
669 to precipitation, resulting in positive surface freshwater forcing and reduced NADW production.
670 Unlike in that study, the mechanism proposed here only invokes changes in stratospheric ozone,
671 not aerosols, and to the best of our knowledge, no study has previously demonstrated an impact of
672 stratospheric ozone changes alone on the AMOC response to a quadrupling of CO₂. Despite the

673 different mechanisms at play, however, our results are generally consistent with those from Rind
674 et al. (2018) in that they highlight the need for renewed focus on surface flux observations to help
675 assess overturning stability.

676 An important caveat with our results is related to known biases in vertical mixing and NADW
677 production in the ocean component of the GISS model (Miller et al. (2021); Romanou et al.
678 (2023)) which likely explain why the low-top version of the coupled atmosphere-ocean climate
679 model (E2.1-G) exhibits a more sensitive AMOC response to a quadrupling of CO₂, compared
680 to some other models (Bellomo et al. (2021)). An important point to highlight, however, is that
681 the high-top model employed in this study is much less sensitive, as the AMOC weakens by ~10
682 SV in response to 4xCO₂, compared to a complete collapse in E2.1-G (see Figure 31 in Rind
683 et al. (2020)). That study showed that this may be related to differences in the parameterization of
684 rainfall evaporation associated with moist convective precipitation, which they show has a strong
685 influence on the AMOC sensitivity in the GISS model via its effect on moisture loading in the
686 atmosphere. While an exhaustive comparison between the models is beyond the scope of this
687 study, the relevant point here is that the 4xCO₂ AMOC response simulated in the E2.2-G NINT
688 ensemble is well within the CMIP5 and CMIP6 ranges documented in Mitevski et al. (2021) (see
689 their Supplementary Figure S3).

690 A natural next step for future research is to examine whether this influence from stratospheric
691 ozone is evident in more realistic scenarios. Although not examined in equal depth, results from the
692 more realistic 1%CO₂ transient simulations also show a greater weakening of the AMOC in OMA,
693 relative to NINT, indicating that the findings presented here are not an artifact of the abruptness
694 of the forcing (not shown). Analysis of the more comprehensive historical and future Shared
695 Socioeconomic Pathway (SSP) (Meinshausen et al. (2020)) integrations is currently underway to
696 identify other factors, including aerosols and the solar cycle (Muthers et al. (2016)), which are
697 likely to influence the ocean circulation. For sake of brevity, however, we reserve further discussion
698 of the more comprehensive results for future work.

699 Finally, our results linking the fast timescale jet response to the ensuing AMOC changes un-
700 derscore the profound impact that changes in lower stratospheric winds alone can have on surface
701 climate, as highlighted in Sigmond and Scinocca (2010). Quite remarkably, our fixed SST and SIC
702 experiments showed that these lower stratospheric wind changes are driven primarily by changes

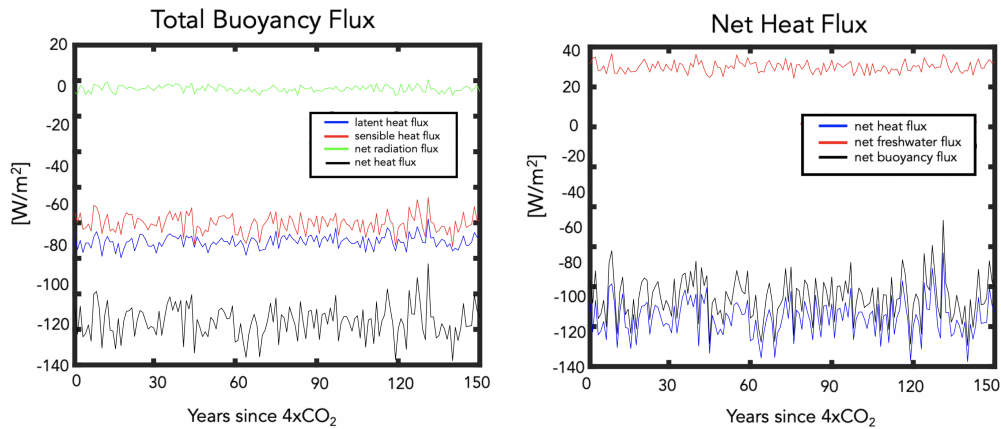
703 in ozone and not by background changes in CO₂ or in sea surface boundary conditions. Taken
704 together, our results suggest that more attention needs to be paid to understanding the time-evolving
705 response of the coupled Earth system to future ozone changes, with a focus on changes in ocean
706 heat transport and how these feed back on the NH jet stream.

707 *Acknowledgments.* C.O. acknowledges helpful discussions with Lettie Roach, Ivan Mitevski
708 and Lorenzo Polvani. G.C. acknowledges support by the SNSF with the “Ambizione” grant
709 N. PZ00P2180043. Climate modeling at GISS is supported by the NASA Modeling, Analysis and
710 Prediction program, and resources supporting this work were provided by the NASA High-End
711 Computing (HEC) Program through the NASA Center for Climate Simulation (NCCS) at Goddard
712 Space Flight Center.

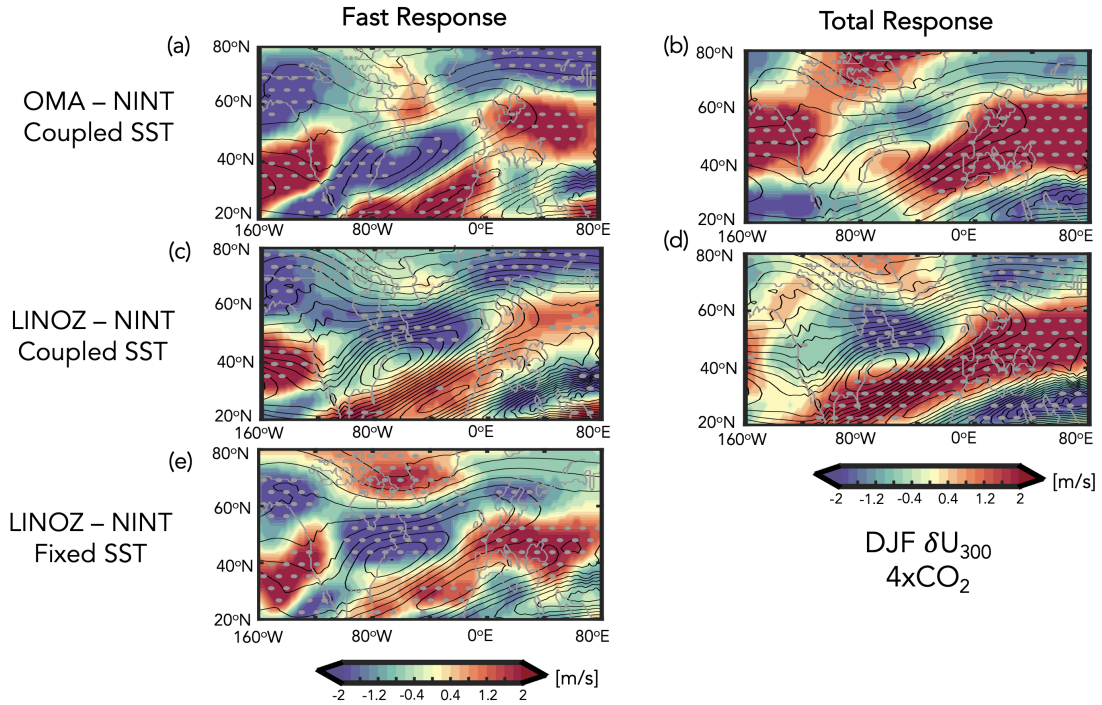
713 *Data availability statement.* The NINT and OMA GISS E2.2-G simulations used in the study
714 are available at the CMIP6 archive via the Earth System Grid Federation ([https://esgf-node.
715 llnl.gov/](https://esgf-node.llnl.gov/)), where NINT and OMA are respectively denoted as “physics version 1” and “physics
716 version 3”. The specific simulations used here are the PiControl, abrupt-2xCO₂, and abrupt-
717 4xCO₂ r1i1p1f1 (NINT) and r1i1p3f1 (OMA) runs. Output needed to reproduce all figures
718 showing the additional three NINT 4xCO₂ simulations, fixed SST simulations as well the four-
719 member LINOZ ensemble is available online at [https://gmao.gsfc.nasa.gov/gmaoftp/
720 corbe/AMOC_Linoz/Data/](https://gmao.gsfc.nasa.gov/gmaoftp/corbe/AMOC_Linoz/Data/). All GISS ModelE components are open source and available at
721 <http://www.giss.nasa.gov/tools/modelE/>.

722 APPENDIX

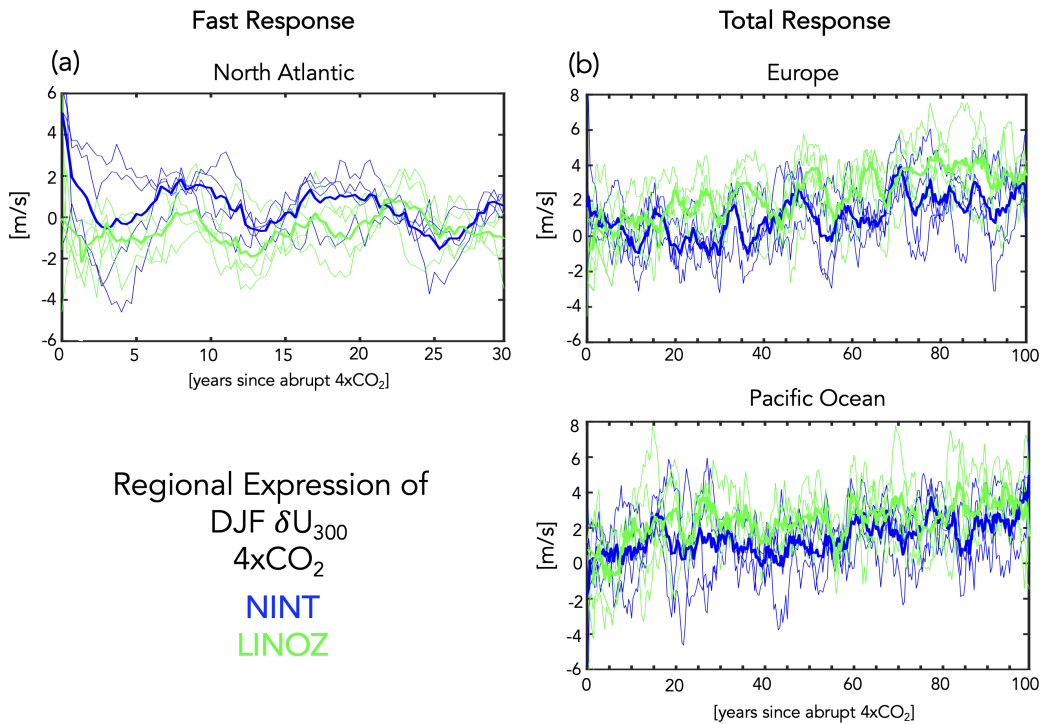
Annual Mean PiControl Climatological
Flux Decompositions over the Irminger Sea



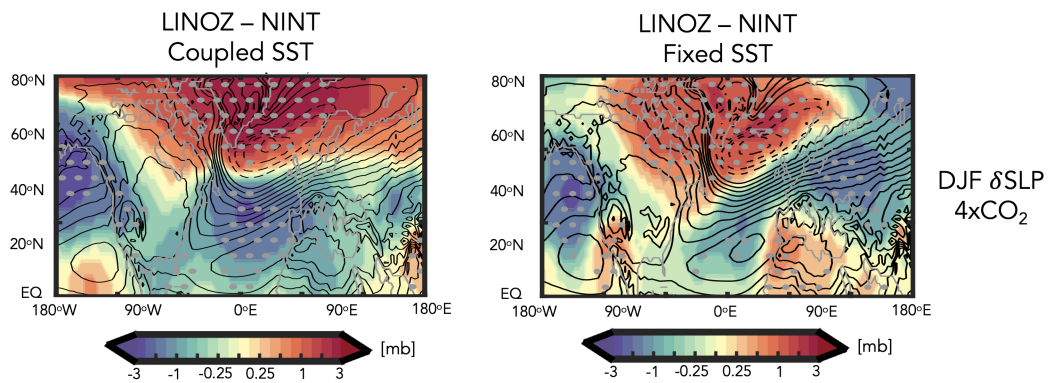
723 FIG. A1. Left: Decomposition of the net surface buoyancy flux (black) into contributions from net heat
 724 (blue) and net freshwater (red) fluxes. Right: Further decomposition of the net surface heat flux (black) into
 725 contributions from latent heat fluxes (Q_E (blue)), sensible heat fluxes (Q_H (red)), and combined solar and
 726 longwave radiative fluxes (Q_S+Q_L (green)). Results are shown for 150 years of the NINT preindustrial control
 727 (PiControl) simulation, evaluated over the Irminger Sea.



728 FIG. A2. Colors show the coupled atmosphere-ocean OMA - NINT (a,b) and LINOZ - NINT (c,d) $4xCO_2$
 729 changes in the DJF 300 hPa zonal winds. One ensemble member is used in the top panels, compared to four
 730 members in the middle row. Panel e shows results from the atmosphere-only ensemble in which the time-evolving
 731 $4xCO_2$ ensemble mean LINOZ ozone response is prescribed and the SSTs, SICs, and background CO_2 are set to
 732 preindustrial values. Left and right panels in the top and middle rows show the responses decomposed into “fast”
 733 (i.e. years 5-20) (a,c) and “total” (i.e. years 100-150) (b,d) responses. Averages over years 40-60 are shown
 734 for the prescribed SST and SIC experiments in panel e, which equilibrate much more rapidly, compared to the
 735 coupled experiments. Black contours denote climatological mean preindustrial control DJF values (U contour
 736 interval: 2 m/s) and stippled regions are statistically significant.



737 FIG. A3. Changes in the DJF zonal winds at 300 hPa, focusing on the “fast” (a) and “total” (b) responses to
 738 4xCO₂, relative to the preindustrial control simulations. The fast response is evaluated over the North Atlantic
 739 (50°W-10°W, 45°N-65°N). The slow response is evaluated over Europe (0°E-80°E, 45°N-65°N) and over the
 740 Pacific (150°E-150°W, 45°N-65°N). Results for the LINOZ and NINT ensembles are shown in green and blue,
 741 respectively (thick lines denote ensemble means).



742 FIG. A4. **Left** panel: Colors show the LINOZ minus NINT ensemble mean difference in the December-
 743 January-February (DJF) “fast” response of the sea level pressure to an abrupt quadrupling of CO₂. Results are
 744 shown for the fully coupled atmosphere-ocean simulations. **Right** panel: The ensemble mean response in sea
 745 level pressure in the experiments in which the time-evolving 4xCO₂ ensemble mean LINOZ ozone response
 746 is prescribed and the SSTs, SICs, and background CO₂ are set to preindustrial values. Black contours denote
 747 climatological mean preindustrial control DJF values (contour interval: 10 mb). Stippled regions are statistically
 748 significant.

749 **References**

- 750 Alexander, M. A., J. D. Scott, and C. Deser, 2000: Processes that influence sea surface temperature
751 and ocean mixed layer depth variability in a coupled model. *Journal of Geophysical Research:
752 Oceans*, **105 (C7)**, 16 823–16 842.
- 753 Ayarzagüena, B., and Coauthors, 2020: Uncertainty in the response of sudden stratospheric
754 warmings and stratosphere-troposphere coupling to quadrupled CO₂ concentrations in CMIP6
755 models. *Journal of Geophysical Research: Atmospheres*, **125 (6)**, e2019JD032 345.
- 756 Baldwin, M. P., and Coauthors, 2021: Sudden stratospheric warmings. *Reviews of Geophysics*,
757 **59 (1)**, e2020RG000 708.
- 758 Bauer, S. E., and Coauthors, 2020: Historical (1850–2014) aerosol evolution and role on climate
759 forcing using the GISS ModelE2. 1 contribution to CMIP6. *Journal of Advances in Modeling
760 Earth Systems*, **12 (8)**, e2019MS001 978.
- 761 Bellomo, K., M. Angeloni, S. Corti, and J. von Hardenberg, 2021: Future climate change shaped
762 by inter-model differences in Atlantic meridional overturning circulation response. *Nature Com-
763 munications*, **12 (1)**, 1–10.
- 764 Bellomo, K., V. L. Meccia, R. D’Agostino, F. Fabiano, S. M. Larson, J. von Hardenberg, and
765 S. Corti, 2023: Impacts of a weakened amoc on precipitation over the euro-atlantic region in the
766 ec-earth3 climate model. *Climate Dynamics*, 1–20.
- 767 Booth, B. B., N. J. Dunstone, P. R. Halloran, T. Andrews, and N. Bellouin, 2012: Aerosols
768 implicated as a prime driver of twentieth-century North Atlantic climate variability. *Nature*,
769 **484 (7393)**, 228–232.
- 770 Butler, A. H., D. W. Thompson, and R. Heikes, 2010: The steady-state atmospheric circulation
771 response to climate change–like thermal forcings in a simple general circulation model. *Journal
772 of Climate*, **23 (13)**, 3474–3496.
- 773 Ceppi, P., and D. L. Hartmann, 2015: Connections between clouds, radiation, and midlatitude
774 dynamics: A review. *Current Climate Change Reports*, **1 (2)**, 94–102.

- 775 Ceppi, P., G. Zappa, T. G. Shepherd, and J. M. Gregory, 2018: Fast and slow components of
776 the extratropical atmospheric circulation response to CO₂ forcing. *Journal of Climate*, **31** (3),
777 1091–1105.
- 778 Chadwick, R., and P. Good, 2013: Understanding nonlinear tropical precipitation responses to co2
779 forcing. *Geophysical research letters*, **40** (18), 4911–4915.
- 780 Chiodo, G., and L. M. Polvani, 2019: The response of the ozone layer to quadrupled CO₂
781 concentrations: Implications for climate. *Journal of Climate*, **32** (22), 7629–7642.
- 782 Chiodo, G., L. M. Polvani, D. R. Marsh, A. Stenke, W. Ball, E. Rozanov, S. Muthers, and
783 K. Tsigaridis, 2018: The response of the ozone layer to quadrupled CO₂ concentrations. *Journal*
784 *of Climate*, **31** (10), 3893–3907.
- 785 Cowan, T., and W. Cai, 2013: The response of the large-scale ocean circulation to 20th century
786 Asian and non-Asian aerosols. *Geophysical Research Letters*, **40** (11), 2761–2767.
- 787 DallaSanta, K., C. Orbe, D. Rind, L. Nazarenko, and J. Jonas, 2021a: Dynamical and trace gas
788 responses of the quasi-biennial oscillation to increased CO₂. *Journal of Geophysical Research:*
789 *Atmospheres*, **126** (6), e2020JD034 151.
- 790 DallaSanta, K., C. Orbe, D. Rind, L. Nazarenko, and J. Jonas, 2021b: Response of the quasi-
791 biennial oscillation to historical volcanic eruptions. *Geophysical Research Letters*, **48** (20),
792 e2021GL095 412.
- 793 Delworth, T. L., and K. W. Dixon, 2000: Implications of the recent trend in the Arctic/North
794 Atlantic oscillation for the North Atlantic thermohaline circulation. *Journal of Climate*, **13** (21),
795 3721–3727.
- 796 Delworth, T. L., and F. Zeng, 2016: The impact of the North Atlantic oscillation on climate
797 through its influence on the Atlantic meridional overturning circulation. *Journal of Climate*,
798 **29** (3), 941–962.
- 799 Delworth, T. L., F. Zeng, L. Zhang, R. Zhang, G. A. Vecchi, and X. Yang, 2017: The central role
800 of ocean dynamics in connecting the North Atlantic oscillation to the extratropical component
801 of the Atlantic multidecadal oscillation. *Journal of Climate*, **30** (10), 3789–3805.

- 802 Eyring, V., S. Bony, G. A. Meehl, C. A. Senior, B. Stevens, R. J. Stouffer, and K. E. Taylor, 2016:
803 Overview of the Coupled Model Intercomparison Project Phase 6 (CMIP6) experimental design
804 and organization. *Geoscientific Model Development*, **9** (5), 1937–1958.
- 805 Garcia, R. R., and W. J. Randel, 2008: Acceleration of the Brewer–Dobson circulation due to
806 increases in greenhouse gases. *Journal of the Atmospheric Sciences*, **65** (8), 2731–2739.
- 807 Gervais, M., J. Shaman, and Y. Kushnir, 2019: Impacts of the North Atlantic warming hole in
808 future climate projections: Mean atmospheric circulation and the North Atlantic jet. *Journal of*
809 *Climate*, **32** (10), 2673–2689.
- 810 Grise, K. M., and L. M. Polvani, 2014: The response of midlatitude jets to increased CO₂:
811 Distinguishing the roles of sea surface temperature and direct radiative forcing. *Geophysical*
812 *Research Letters*, **41** (19), 6863–6871.
- 813 Grise, K. M., and L. M. Polvani, 2016: Is climate sensitivity related to dynamical sensitivity?
814 *Journal of Geophysical Research: Atmospheres*, **121** (10), 5159–5176.
- 815 Isaksen, I. S., and Coauthors, 2009: Atmospheric composition change: Climate–chemistry inter-
816 actions. *Atmospheric Environment*, **43** (33), 5138–5192.
- 817 Jackson, L., R. Kahana, T. Graham, M. Ringer, T. Woollings, J. Mecking, and R. Wood, 2015:
818 Global and european climate impacts of a slowdown of the amoc in a high resolution gcm.
819 *Climate dynamics*, **45**, 3299–3316.
- 820 Kantha, L. H., and C. A. Clayson, 2000: *Small scale processes in geophysical fluid flows*. Elsevier.
- 821 Kelley, M., and Coauthors, 2020: GISS-E2. 1: Configurations and climatology. *Journal of Ad-*
822 *vances in Modeling Earth Systems*, **12** (8), e2019MS002 025.
- 823 Khatri, H., R. G. Williams, T. Woollings, and D. M. Smith, 2022: Fast and slow subpolar ocean
824 responses to the North Atlantic oscillation: Thermal and dynamical changes. *Geophysical*
825 *Research Letters*, **49** (24), e2022GL101 480.
- 826 Li, F., and P. A. Newman, 2022: Prescribing stratospheric chemistry overestimates southern hemi-
827 sphere climate change during austral spring in response to quadrupled CO₂. *Climate Dynamics*,
828 1–18.

- 829 Lindzen, R. S., 1987: On the development of the theory of the QBO. *Bulletin of the American*
830 *Meteorological Society*, 329–337.
- 831 Liu, W., A. V. Fedorov, S.-P. Xie, and S. Hu, 2020: Climate impacts of a weakened Atlantic
832 meridional overturning circulation in a warming climate. *Science Advances*, **6** (26), eaaz4876.
- 833 Ma, L., T. Woollings, R. G. Williams, D. Smith, and N. Dunstone, 2020: How does the winter
834 jet stream affect surface temperature, heat flux, and sea ice in the North Atlantic? *Journal of*
835 *Climate*, **33** (9), 3711–3730.
- 836 Marshall, J., H. Johnson, and J. Goodman, 2001: A study of the interaction of the North Atlantic
837 oscillation with ocean circulation. *Journal of Climate*, **14** (7), 1399–1421.
- 838 McLinden, C., S. Olsen, B. Hannegan, O. Wild, M. Prather, and J. Sundet, 2000: Stratospheric
839 ozone in 3-D models: A simple chemistry and the cross-tropopause flux. *Journal of Geophysical*
840 *Research: Atmospheres*, **105** (D11), 14 653–14 665.
- 841 Meinshausen, M., and Coauthors, 2020: The shared socio-economic pathway (SSP) greenhouse
842 gas concentrations and their extensions to 2500. *Geoscientific Model Development*, **13** (8),
843 3571–3605.
- 844 Menzel, M. E., D. Waugh, and K. Grise, 2019: Disconnect between hadley cell and subtropical jet
845 variability and response to increased co2. *Geophysical Research Letters*, **46** (12), 7045–7053.
- 846 Meraner, K., S. Rast, and H. Schmidt, 2020: How useful is a linear ozone parameteriza-
847 tion for global climate modeling? *Journal of Advances in Modeling Earth Systems*, **12** (4),
848 e2019MS002 003.
- 849 Miller, R. L., and Coauthors, 2021: Cmp6 historical simulations (1850–2014) with GISS-E2. 1.
850 *Journal of Advances in Modeling Earth Systems*, **13** (1), e2019MS002 034.
- 851 Mitevski, I., C. Orbe, R. Chemke, L. Nazarenko, and L. M. Polvani, 2021: Non-monotonic
852 response of the climate system to abrupt CO₂ forcing. *Geophysical Research Letters*, **48** (6),
853 e2020GL090 861.

854 Muthers, S., C. C. Raible, E. Rozanov, and T. F. Stocker, 2016: Response of the AMOC to reduced
855 solar radiation—the modulating role of atmospheric chemistry. *Earth System Dynamics*, **7** (4),
856 877–892.

857 Nowack, P. J., N. Luke Abraham, A. C. Maycock, P. Braesicke, J. M. Gregory, M. M. Joshi,
858 A. Osprey, and J. A. Pyle, 2015: A large ozone-circulation feedback and its implications for
859 global warming assessments. *Nature Climate Change*, **5** (1), 41–45.

860 O’Callaghan, M. J. D. S., Ameen, and D. Mitchell, 2014: The effects of different sudden stratospheric
861 warming types on the ocean. *Geophysical Research Letters*, **41** (21), 7739–7745.

862 Orbe, C., and Coauthors, 2020: GISS Model E2.2: A climate model optimized for the middle
863 atmosphere—2. Validation of large-scale transport and evaluation of climate response. *Journal*
864 *of Geophysical Research: Atmospheres*, **125** (24), e2020JD033 151.

865 Orbe, C., and Coauthors, 2023: Atmospheric response to a collapse of the North Atlantic circulation
866 under a mid-range future climate scenario: A regime shift in Northern Hemisphere dynamics.
867 *Journal of Climate*.

868 Reichler, T., J. Kim, E. Manzini, and J. Kröger, 2012: A stratospheric connection to Atlantic
869 climate variability. *Nature Geoscience*, **5** (11), 783–787.

870 Rind, D., J. Jonas, N. Balachandran, G. A. Schmidt, and J. Lean, 2014: The QBO in two GISS global
871 climate models: 1. Generation of the QBO. *Journal of Geophysical Research: Atmospheres*,
872 **119** (14), 8798–8824.

873 Rind, D., G. A. Schmidt, J. Jonas, R. Miller, L. Nazarenko, M. Kelley, and J. Romanski, 2018:
874 Multicentury instability of the Atlantic meridional circulation in rapid warming simulations with
875 GISS ModelE2. *Journal of Geophysical Research: Atmospheres*, **123** (12), 6331–6355.

876 Rind, D., R. Suozzo, N. Balachandran, A. Lacis, and G. Russell, 1988: The GISS global climate-
877 middle atmosphere model. Part I: Model structure and climatology. *Journal of the Atmospheric*
878 *Sciences*, **45** (3), 329–370.

879 Rind, D., and Coauthors, 2020: GISS Model E2.2: A climate model optimized for the mid-
880 dle atmosphere—model structure, climatology, variability, and climate sensitivity. *Journal of*
881 *Geophysical Research: Atmospheres*, **125** (10), e2019JD032 204.

- 882 Roach, L. A., E. Blanchard-Wrigglesworth, S. Ragen, W. Cheng, K. C. Armour, and C. M. Bitz,
883 2022: The impact of winds on AMOC in a fully-coupled climate model. *Geophysical Research*
884 *Letters*, e2022GL101203.
- 885 Robson, J., and Coauthors, 2022: The role of anthropogenic aerosol forcing in the 1850–1985
886 strengthening of the amoc in cmip6 historical simulations. *Journal of Climate*, **35** (20), 6843–
887 6863.
- 888 Romanou, A., and Coauthors, 2023: Stochastic bifurcation of the North Atlantic circulation under
889 a mid-range future climate scenario with the NASA-GISS ModelE. *Journal of Climate*.
- 890 Shaw, T., and Coauthors, 2016: Storm track processes and the opposing influences of climate
891 change. *Nature Geoscience*, **9** (9), 656–664.
- 892 Shaw, T. A., 2019: Mechanisms of future predicted changes in the zonal mean mid-latitude
893 circulation. *Current Climate Change Reports*, **5** (4), 345–357.
- 894 Shepherd, T. G., 2014: Atmospheric circulation as a source of uncertainty in climate change
895 projections. *Nature Geoscience*, **7** (10), 703–708.
- 896 Sigmond, M., and J. F. Scinocca, 2010: The influence of the basic state on the Northern Hemisphere
897 circulation response to climate change. *Journal of Climate*, **23** (6), 1434–1446.
- 898 Simpson, I. R., T. A. Shaw, and R. Seager, 2014: A diagnosis of the seasonally and longitudinally
899 varying midlatitude circulation response to global warming. *Journal of the Atmospheric Sciences*,
900 **71** (7), 2489–2515.
- 901 Smith, D. M., and Coauthors, 2019: The polar amplification model intercomparison project
902 (PAMIP) contribution to CMIP6: Investigating the causes and consequences of polar amplifica-
903 tion. *Geoscientific Model Development*, **12** (3), 1139–1164.
- 904 Swingedouw, D., P. Ortega, J. Mignot, E. Guilyardi, V. Masson-Delmotte, P. G. Butler, M. Khodri,
905 and R. S  ferian, 2015: Bidecadal North Atlantic ocean circulation variability controlled by
906 timing of volcanic eruptions. *Nature Communications*, **6** (1), 1–12.

- 907 Vallis, G. K., P. Zurita-Gotor, C. Cairns, and J. Kidston, 2015: Response of the large-scale structure
908 of the atmosphere to global warming. *Quarterly Journal of the Royal Meteorological Society*,
909 **141 (690)**, 1479–1501.
- 910 Visbeck, M., H. Cullen, G. Krahnemann, and N. Naik, 1998: An ocean model’s response to North
911 Atlantic oscillation-like wind forcing. *Geophysical Research Letters*, **25 (24)**, 4521–4524.
- 912 Voigt, A., and T. A. Shaw, 2015: Circulation response to warming shaped by radiative changes of
913 clouds and water vapour. *Nature Geoscience*, **8 (2)**, 102–106.
- 914 Yuval, J., and Y. Kaspi, 2020: Eddy activity response to global warming–like temperature changes.
915 *Journal of Climate*, **33 (4)**, 1381–1404.
- 916 Zhai, H. L. J., Xiaoming, and D. P. Marshall, 2014: A simple model of the response of the Atlantic
917 to the North Atlantic oscillation. *Journal of Climate*, **27 (11)**, 4052–4069.
- 918 Zhang, R., R. Sutton, G. Danabasoglu, Y.-O. Kwon, R. Marsh, S. G. Yeager, D. E. Amrhein, and
919 C. M. Little, 2019: A review of the role of the atlantic meridional overturning circulation in
920 atlantic multidecadal variability and associated climate impacts. *Reviews of Geophysics*, **57 (2)**,
921 316–375.
- 922 Zhang, R., and Coauthors, 2013: Have aerosols caused the observed atlantic multidecadal vari-
923 ability? *Journal of the Atmospheric Sciences*, **70 (4)**, 1135–1144.
- 924 Zhang, X., D. Waugh, and C. Orbe, 2023: Response of tropospheric transport to abrupt CO₂ in-
925 crease: Dependence on the Atlantic Meridional Overturning Circulation. *Journal of Geophysical*
926 *Research: Atmospheres*.